UNIVERSITÄT FÜR BODENKULTUR WIEN
University of Natural Resources and Life Sciences, Vienna

H75 Department of Food Sciences and Technology
Food Biotechnology Laboratory

Pre steady-state studies on recombinant *Myriococcum thermophilum* cellobiose dehydrogenase and surface-charge variants

Master thesis submitted by Bernadette Serro

Supervised by Priv.-Doz. Dr. Clemens Karl Peterbauer

Vienna, October 2010

The journey is the reward.

Acknowledgement

I dedicate this work to my parents and my beloved triplet sisters Christine and Stefanie.

I want to thank Univ.Prof. Dipl.-Ing. Dr. Dietmar Haltrich and Priv.-Doz. Dr. Clemens Karl Peterbauer for giving me the opportunity to conduct research for my master thesis at the Food Biotechnology Laboratory, Department of Food Sciences and Technology at the University of Natural Resources and Life Sciences, Vienna.

I would like to show my gratitude to Dipl.-Ing. Dr. Roland Ludwig for his support and patience and for guiding me through my research. Special thanks go to Dipl.-Ing. Dr. Wolfgang Harreither and Dipl.-Ing. Kawah Zahma, both of them were giving me practical advices and thus contributing to an encouraging work environment. Sincere thanks are given to all who shared my work experience with me, be it in the lab or outside.

Abstract

Cellobiose dehydrogenase (CDH) is secreted by ascomycete and basidiomycetes fungi and catalyzes the oxidation of sugars. Its native substrate is cellobiose, a β-1,4-linked disaccharide forming cellulose, thus, making CDH and important player in the biodegradation of wood. In this process, the oxidation of the natural substrate cellobiose is followed by the reduction of quinones and re-oxidation of the enzyme. CDH is the only known extracellular flavocytochrome to date, consisting of an N-terminal cytochrome domain which is connected via a linker to a larger C-terminal flavodehydrogenase domain.

Heterologous expression of *Myriococcum thermophilum* CDH from in *Pichia pastoris* and its purification were core elements of this study. The highly purified enzyme with a ratio A_{420}/A_{280} of 0.64 was then subjected to pre steady-state analysis. This technique allows the direct determination of intramolecular electron transfer (IET), measured by the rate constant for heme *b* reduction. The kinetic constants K_d and k_{lim} for cellobiose, lactose, glucose and maltose were determined. The catalytic efficiency of the heme *b* reduction process for glucose is outstanding, showing 3.2-fold higher value as with the natural substrate cellobiose. Highest observed rate constant of the heme *b* was 0.93 s^{-1} at pH 4.0, whereas for FAD the highest observed rate constant was 38.0 s^{-1} at pH 7.0. The variants D547K/E550K and D547K/E550K/E603K were found to be the most promising surface-charge variants, as they exhibit satisfying reduction performance of FAD with outstanding heme *b* rate constants at pH 7.5.

As the surface-charge variants of CDH from *Myriococcum thermophilum* showed little glucose discrimination and outstanding reduction rates for heme *b*, they are facilitating direct electron transfer (DET) between the redox center of an enzyme and a polarized electrode and, thus, have the potential to be used in third generation biosensors.

Zusammenfassung

Cellobiose Dehydrogenase (CDH) katalysiert die Oxidation von Zuckern, insbesondere von Disaccharide die β-1,4 glykosidisch miteinander verknüpft sind. Das natürliche Substrat welches von CDH oxidiert wird ist Cellobiose, wodurch die CDH zwei Elektronen aufnimmt und durch die Abgabe dieser an Chinone re-oxidiert wird. Schlauchpilze (Ascomycota) und Basidienpilze (Basidiomycota) welche CDH bilden und in ihre Umgebung sekretieren, spielen daher eine wichtige Rolle beim Abbau von biologischem Material. CDH ist bisher das einzig bekannte extrazelluläre Flavohaemenzym, wobei die am N-terminalen Ende ein Cytochrome *b* Domäne über eine Linker-Sequenz mit dem größeren am C-terminale befindliche Flavodehydrogenase Domäne verbunden ist.

CDH aus dem Wildtypstamm von *Myriococcum thermophilum* wurde rekombinant in *Pichia pastoris* hergestellt. Nach einem 3-stufigen Reinigungsverfahren wurde das Enzym mit der Reinheitszahl (A_{420}/A_{280}) von 0.64 für Pre steady-state Experiment herangezogen. Die Haem *b* – Rate beschreibt dabei direkt den Intramolekularen Elektronentransfers (IET). Die kinetischen Konstanten K_d and k_{lim} für Cellobiose, Laktose, Glukose und Maltose wurden ermittelt und miteinander verglichen. Der k_{lim} / K_d Quotient (katalytische Effizienz) der Haem *b* – Rate für Glukose war 3.2-fach höher als für Cellobiose. Das pH Optimum für die Reduktion von Haem *b* lag bei pH 4.0 (0.93 s^{-1}), für die Flavodehydrogenase bei pH 7.0 (38.0 s^{-1}). Die Enzymvarianten der Mutationen D547K/E550K und D547K/E550K/E603K hatten nach Mischen mit dem Substrat Glukose bei pH 7.5, herausragende Haem *b* – Raten bei zufriedenstellende Reduktionsraten von Flavodehydrogenase.

Durch die Oberflächenladungsänderungen von CDH Mutanten von *Myriococcum thermophilum*, wurde die Umsetzung der Glukose, gemessen an der Haem *b* – Rate, erheblich gesteigert. Die oben genannten Enzymvarianten sind daher potentielle Anwärter für Biosensoren der Dritten Generation, da sie den Direkten Elektronentransfer (DET) zwischen Redox-Zentrum des Enzyms und einer polarisierten Elektrode, fördern.

Table of contents

Table of figures

List of tables

List of abbreviations

AEC	Anion exchange chromatography
CBM	Carbohydrate-binding module
CDH	Cellobiose dehydrogenase
cyt *c*	Cytochrome *c*
Da	Dalton (unit of molecular mass)
DCIP	2,6-dichloroindophenol
DET	Direct electron transfer
DO	Dissolved oxygen
E	Enzyme
E.C.	Enzyme Commission
ES	Enzyme-substrate complex
FAD	Flavin adenine dinucleotide
$\Delta G^{\ddagger}$	Free energy of activation in enzyme catalyzed reactions
HIC	Hydrophobic interaction chromatography
IET	Intramolecular electron transfer
k_1	Rate constant of forming ES from E + S
k_2	Rate constant of dissociation of ES into E + S
k_3	Rate constant of forming P + E from ES
K_M	Michaelis-Menten constant
P	Product
rec*Mt*CDH	recombinant *Myriococcum thermophilum* CDH
rec*Pc*CDH	recombinant *Phanerochaete chrysosporium* CDH
S	Substrate
V_0	Reaction velocity
V_{max}	Maximum reaction velocity

1 Introduction

1.1 Aims of the study and biotechnological implications

Heterologous expression and purification of CDH from *Myriococcum thermophilum* (CBS 208.89) in *Pichia pastoris* (X-33) were core elements within the scope of this study. The highly purified enzyme with a ratio A_{420}/A_{280} of 0.64 was then subject of pre steady-state analysis with varying pH in the range of 3.0 to 7.5 and different carbohydrates as substrates, e. g. cellobiose, lactose, glucose and maltose, at constant temperature, allowing determination of pH optima and substrate discrimination. Pre steady-state measurements were also conducted with the *Myriococcum thermophilum* CDH surface-charge variants, D547K, E550K, D547K/E550K, D547K/E550K/E603K and D297K/D547K/E550K/E603K, in order to evaluate the termination of repulsive electrical forces and its effects on the IET. Pre steady-state kinetic measurements should also clarify the interplay between the two redox domains during electron transfer which is yet not fully elucidated. Additionally, stopped-flow measurements with recombinant wild-type CDH and its deglycosylated preparation from *Phanerochaete chrysosporium* (*Pc*CDH) were carried out to elucidate the importance of glycosyl-residues on IET and to compare with *Mt*CDH.

When IET is high, which is determined by the rate constant for heme *b* reduction, high responses in the current are achieved. This property is useful for DET in the third generation of biosensors. Such systems have sensor and transducer joint in one component and are immobilized on the surface of an electrode. Electrons are directly shuttled between the redox center of an enzyme and a polarized electrode, thus, increasing electron sensitivity. The operation in a potential window close to the redox potential of the enzyme makes the system less susceptible to interfering reactions, thus, as a second outstanding feature for third generation of biosensors, increasing selectivity.

CDH originating from *Myriococcum thermophilum* is of special biotechnological interest in the field of amperometric biosensors as it shows higher temperature optimum and glucose conversion with high reduction rates for heme *b*. Thus, CDH from *Myriococcum thermophilum* cannot only exclusively be applied as a lignocelluloses degrading or bioremediation agent, but also has the potential acting as a promising tool in the medical-diagnostic area and in microbial fuel cells.

1.2 Wood biodegradation

Lignocellulosic biomass composed of cellulose and hemicelluloses bound to and framed by lignin is eventually decomposed to humus within the global carbon cycle in a microbiological digestion process, releasing carbon dioxide and heat. The interplay of microorganisms such as bacteria, actinomycetes and fungi within a distinct time frame and under certain circumstances met, allows a closed cycle of natural resources and energy by the organisms involved; in particular the recycling of plant biomass and the important role of saprophytes. Important factors such as C/N ratio, moisture, temperature and pH, vary along the decomposition process at different stages and constitute a distinct microorganism population at each stage. A natural composting process had been described by Crawford et al. (1) and Tuomela et al. (2) where pH changes from approximately 5.0 to 7.5 occur along the decomposition process, while the temperature profile shows an inverted parabola, beginning in mesophilic and peaking into thermophilic microclimate and eventually followed by cooling and maturation phase, whereas the temperature ranges from approximately 10°C to 65°C.

Maheshwari et al. (3) investigated thermophilic fungi and their enzymes reporting that *Myriococcum thermophilum* has an optimal growth temperature of 45°C and an upper temperature limit of 53°C and that it is a producer of cellobiose dehydrogenase (CDH; E.C. 1.1.99.18; cellobiose:acceptor 1-oxidoreductase). This fungal enzyme is an oxidoreductase acting as an electron acceptor by oxidizing the reducing end of carbohydrates; thus, CDH had been found to take part in the degradation process of lignin and cellulose. Most research to date concentrated on white-rot fungi, which are capable of mineralizing lignin, visible as whitening or bleaching of the wooden substrate. White-rot fungi belong to the phyla basidiomycota. Cameron et al. (4) showed that CDH generates Fenton-based hydroxyl radicals when Fe^{3+} acts as the electron acceptor and suggested a model for lignin degradation. Li et al. (5) and Moukha et al. (6) reported upregulation of the *cdh* in cellulose-containing media, whereas secretion of CDH mainly occurs during the exponential growth-phase (7), indicating that cellulose is the main carbon source used by white-rot fungi. CDH activity as a research field in biochemistry, the oxidation of the natural substrate cellobiose and the following reduction of quinones and re-oxidation of the enzyme in particularly, was first discovered by Westermark and Eriksson in 1974 (8). CDH is the currently only known extracellular flavocytochrome (9) and secreted by both, basidiomycota and ascomycota. The working group of Divne was able to determine the crystal structure of the separated *b*-type cytochrome (9) and flavodehydrogenase (10) domains of CDH from *Phanerochaete chrysosporium*. The *b*-type cytochrome domain at the N-terminus is

connected via a linker to a larger C-terminal flavodehydrogenase domain. Zámocký et al. (11) gives a comprehensive review of selected fungi secreting the flavocytochrome, and reveal different pH and temperature optima within the fungal species.

1.3 Catalysis and enzyme kinetics

Here, only the basic key elements of enzyme thermodynamic and kinetics shall be given. For a start, the reader is encouraged to delve into the works of Berg et al. (12) and Price et al. (13).

In any chemical reaction taking place, the free energy difference (ΔG) between the reactants and products accounts for the reaction equilibrium, in other words, the direction in which the reaction will go. Enzymes accelerate the reaction but do not alter the equilibrium itself. Any chemical reaction of a substrate S to form the product P goes through a transition state $S^{‡}$ that has a higher free energy than either S or P does. As the transition state $S^{‡}$ has the highest free energy throughout the reaction, it is also the most seldom occupied species along the reaction pathway. The difference in free energy between the transition state and the substrate is also known as activation energy $\Delta G^{‡}$. Note that enzymes do not alter ΔG, instead they lower the activation energy $\Delta G^{‡}$ by binding the substrate, or in other words, enzymes facilitate the formation of the transition state. Thus, the bound substrate to the enzyme creates a new reaction pathway whose transition state energy is lower than that of the reaction in the absence of enzyme (Figure 1).

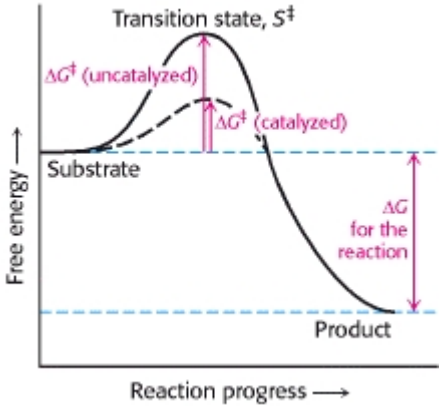

Figure 1. Energy profile comparing an uncatalyzed and catalyzed reaction. Reference: **(12)**

The evidence of the formation of such an ES complex can be seen in reaching a maximum rate constant with increasing substrate concentration until equilibrium. The state-of-the-art

techniques used to investigate enzyme catalyzed reactions are X-ray crystallographic and spectroscopic techniques. The end product of the former is a 3D-structure of the enzyme in its transition state. The latter is based on the absorption difference upon catalyzed reactions, as the formation of an ES complex differs in its spectroscopic characteristics from the unbound substrate and free enzyme (further see 1.7). The essence of enzymatic catalysis lies in the specific binding of the transition state, meaning that an enzyme often catalyzes only a single reaction in a stereoselective manner. Selective and specific in the used sense mean that enzymes select their substrates and carry out the reaction stereoselectively on the substrate to form the product. They enhance the reaction rate of 10^6 to 10^{14} compared to the uncatalyzed rate. The reaction rate of very efficient enzyme-substrate complexes is often limited only by diffusion, approximately 10^8 to 10^9 s^{-1} M^{-1}. As enzymes are proteins, they also have a range of properties not normally associated with catalysis, such as their ability to respond to external signals or to their environment. Classification of enzymes is done according to the reaction they catalyze (Table 1).

Table 1. The six enzyme classes. Reference: **(13)**

	Class of enzyme	**Type of reaction**
1	Oxidoreductases	Catalyze redox reactions in which one substrate is reduced at the expense of a second that is oxidized
2	Transferases	Catalyze reactions in which a group is transferred from one substrate to another
3	Hydrolases	Catalyze reactions in which a substrate is hydrolyzed
4	Lyases	Catalyze reactions in which a group is eliminated from a substrate to form a double bond
5	Isomerases	Catalyze isomerisation reactions
6	Ligases	Catalyze the joining together of two molecules at the expense of ATP, or some other free energy source

Steady-state kinetics gives only limited information on a multistep enzymatic reaction. An enzymatic reaction such as shown in equation 1 involves six reaction constants but is described only by two Michaelis-Menten parameters (V_{max} and K_M) (Figure 3). Thus, studies on steady-state kinetics only describe the substrate-enzyme complex by investigating the rate-determining step at very low substrate concentrations. In order to describe the enzyme itself by investigating all rate constants and intermediates involved, different models have been established to describe the early reactions of enzymatic turnover until steady-state is reached. Nevertheless, a brief

description on the model of Leonor Michaelis and Maud Menten (1913) will be given first, as it is crucial for understanding enzyme kinetics.

$$E + S \underset{k_{-1}}{\overset{k_1}{\rightleftarrows}} ES \xrightarrow{k_2} E + P \qquad (1)$$

$$V_0 = V_{\max} \frac{[S]}{[S] + K_M} \qquad (2)$$

$$E + S \underset{k_{-1}}{\overset{k_1}{\rightleftarrows}} ES \underset{k_{-2}}{\overset{k_2}{\rightleftarrows}} EP \underset{k_{-3}}{\overset{k_3}{\rightleftarrows}} E + P \qquad (3)$$

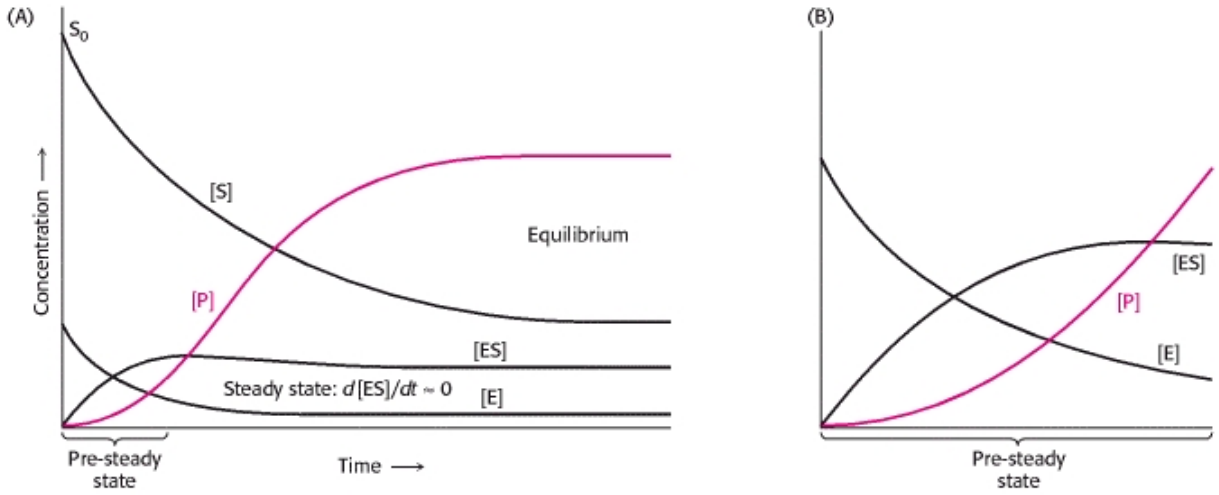

Figure 2. Changes in the concentration of reaction participants of an enzyme-catalyzed reaction with time. (A) Steady-state conditions. **(*B*)** Pre steady-state conditions. Reference: **(12)**

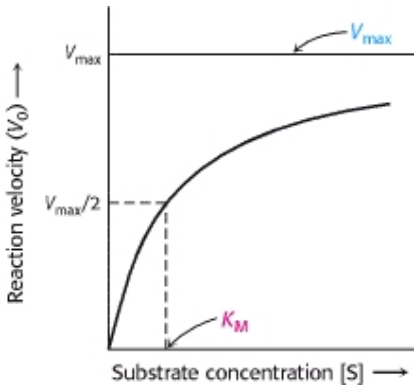

Figure 3. Michaelis-Menten kinetics. Reaction velocity versus substrate concentration in an enzyme-catalyzed reaction. Reference: **(12)**

The Michaelis-Menten equation accounts for the kinetic data given in Figure 3. At very low substrate concentration, when [S] << KM, it gives equation 4. The rate is directly proportional to the substrate concentration (first order). While at high substrate concentration, when [S] >> KM, the following relationship is derived $V_0 = V_{max}$, i.e. the rate is maximal and independent of substrate concentration (zero order).

$$V_0 = \frac{V_{max}}{K_M}[S] \qquad (4)$$

The Michaelis constant K_M, is under certain circumstances identical to the dissociation constant (K_d), is equal to the substrate concentration at which the reaction rate is half its maximal value, when [S] = K_M; or in other words, the K_M value is the concentration of substrate at which half the active sites of an enzyme are filled. Consequently, the knowledge of the K_M value of an enzyme towards a particular substrate gives information on the approximation of substrate concentration *in vivo*. Moreover, the K_M value is related to the rate constants of the individual steps in the catalytic reaction, as follows

$$K_M = \frac{k_{-1} + k_2}{k_1} \qquad (5)$$

$$[ES] = \frac{[E][S]}{K_M}, \text{ where: } [E] = [E]_T - [ES] \qquad (6)$$

The concentration of uncombined enzyme E is equal to the total enzyme concentration $[E]_T$ minus the concentrate of the ES complex. Considering a limiting case where the ES complex dissociates to E and S much more rapidly than product is formed, i. e. $k_{-1} >> k_2$; and $K_M = \frac{k_{-1}}{k_1}$.

In this particular case, the K_M is equal to the dissociation constant of the ES complex, as can be easily followed by equation 1; where a high K_M indicates weak binding and a low K_M indicates strong binding. Again, it must be stressed that K_M only indicates the affinity of the ES complex when the dissociation rate k_{-1} is much greater than the product release rate k_2. Thus, the Michaelis constant K_M is an important characteristic of an enzyme-catalyzed reaction and is significant for its biological function. Most enzymes exhibit a K_M value in the range of 10^{-2} and 10^{-7} M. Beside on the substrate converted, the K_M value for an enzyme depends on environmental conditions such as pH, temperature and ionic strength.

The maximum rate V_{max} is the maximum turnover number of an enzyme, which is defined as the number of substrate molecules converted into product by an enzyme molecule in a unit time when the enzyme is fully saturated with substrate. V_{max} is equal to the kinetic constant k_2, also often called k_{cat} or k_{lim}. If the concentration of active sites of the enzyme $[E]_T$ is known, V_{max} reveals the turnover number, where $V_{max} = k_2[E]_T$. Maximal rate (V_{max}) is attained when the catalytic sites on the enzyme are saturated with substrate, i.e. $[ES] = [E]_T$.

Under physiological conditions, most enzymes are normally not saturated with substrate; or in other words most of the active sites in the enzyme are unoccupied, as substrate concentration in cellular systems is rather low compared to the K_M value, i.e. $[S] / K_M$ is found to be in between 0.01 to 1.0. The catalytic efficiency number characterizes the kinetics of an enzyme under these typical cellular conditions, where $[S] << K_M$. Combining equation 7, assuming that the catalytic rate is equal to the ES complex concentration, and equation 6 under the assumption that $[S] << K_M$, meaning that the concentration of free enzyme E is nearly equal to the total concentration of enzyme E_T, gives equation 8.

$$V_0 = k_2[ES] \quad (7)$$

$$V_0 = \frac{k_{cat}}{K_M}[S][E]_T \quad (8)$$

Under physiological substrate concentration, the reaction rate V_0 thus depends on the values of the catalytic efficiency k_{cat}/K_M, substrate concentration [S] and total concentration of enzyme $[E]_T$. Thus, the k_{cat}/K_M value is the rate constant for the interaction of substrate and enzyme and a measure of catalytic efficiency. By comparing catalytic efficiencies of various substrates towards an enzyme, the enzyme's preference for a particular substrate can be elucidated; thus, giving estimations on the most probable natural substrate for a particular enzyme. The catalytic efficiency is restricted by the rate determining step, which is set by k_1, the rate of formation of the ES complex. This rate cannot be faster than the diffusion-controlled encounter of an enzyme with its substrate, i.e. between 10^8 and 10^9 s^{-1} M^{-1}. The only way to increase catalytic efficiency is by decreasing the time for diffusion, which itself is dependent on the encounter of the substrate with the active site of the enzyme. Often electric forces on the enzyme attract and facilitate the encounter with the substrate, thus enhancing catalytic efficiency. This is crucial when designing surface-charge variants showing high catalytic efficiencies with a particular substrate.

In contrast to the steady-state kinetics under Michaelis-Menten assumptions which describe the enzymatic reaction at steady-state, pre steady-state kinetics give information on the reaction before steady-state is reached (Figure 2, (*B*)). Here, a brief overview of a first order and second order process is given. The reader is encouraged to consult Wilson and Torres (14) to gain more detailed insight in this topic.

Often, reactions of the form shown in equation 9 follow a first-order process with an exponential time course. A mathematical description of such a process is given by equation 10, where the observed rate constant $k_{obs} = k_1 + k_{-1}$; k_1 and $k_{-1}$are the first-order rate constants and have units s^{-1} and the equilibrium constant $K = k_1/k_{-1}$. Where the equilibrium lies far to the right, the value of k_{-1} may be ignored and $k_{obs} \approx k_1$. The absorbance changes upon catalysis are used to monitor the reaction, as absorbance and the concentrations are linearly related described by Beer-Lambert law, which reads as follows $\Delta A = \Delta\varepsilon \cdot c \cdot l$.

$$A \underset{k_{-1}}{\overset{k_1}{\rightleftharpoons}} B \qquad (9)$$

$$[A] = [A]_0 e^{-(k_{obs})t} \qquad [B] = [A]_0 (1 - e^{-(k_{obs})t}) \qquad (10)$$

Other reactions show a second-order process, such as shown in equation 11. Integration of the rate equations involved here is complex and global analysis is used to retrieve the rate constants. It must be pointed out that using the fitting program provided with the apparatus is using the measured absorbance values and not the concentration of the reactants. Thus, the second-order rate constants will have the units of $\Delta A^{-1}\ s^{-1}$ and thus must be converted by the appropriate $\Delta\varepsilon_\lambda$ to $M^{-1}\ s^{-1}$.

$$A + B \underset{k_{-1}}{\overset{k_1}{\rightleftharpoons}} C \qquad \text{or} \qquad A + B \underset{k_{-1}}{\overset{k_1}{\rightleftharpoons}} C + D \qquad (11)$$

If conducting the experiment under conditions where one of the reactants, say A, is in large excess (>10-fold) over the products P, the equation may be simplified to equation 12. Under so called pseudo-first-order processes, the component in excess can be considered to remain constant. The observed rate constant k_{obs} is then called pseudo-first-order rate constant.

$$[P] = [B]_0 (1 - e^{-(k_{obs})t}) \qquad k_{obs} = k_1 [A_0] \qquad (12)$$

Under pseudo-first-order conditions where one of the reactants, say A, is in large excess over the other, say *B*; reversible second-order reactions also yield the same exponential forms as above,

but also depends on the initial concentration of the reactant in excess (equation 13). Determining the rate constant k_1 can be easily achieved by measuring the k_{obs} at a number of concentrations of the reactant in excess.

$$k_{obs} = k_1[A_0] + k_{-1} \qquad (13)$$

1.4 Stopped-flow spectrophotometry

For measuring pre steady-state kinetics, a stopped-flow spectrophotometer is one of the preferred technical devices (Figure 4). After the rapid mixture of two reactants, e.g. substrate and enzyme, followed by the transfer of this resulting mixture (100-150 µL in standard instruments) to an optical cell (20 µL in standard instruments), where the reaction is monitored. In state-of-the-art instruments, the elapsing time from pushing the plunger (pneumatically driven, 10 bar) to first detection of reaction should be approximately 1 ms.

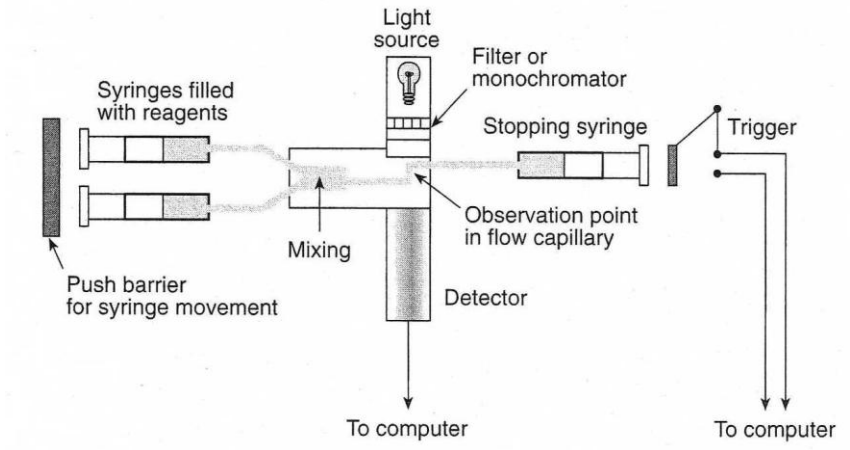

Figure 4. Schematic diagram of a conventional stopped-flow spectrophotometer. Reference: **(14)**

The physical description of a stopped-flow measurement is described as follows; the two reactants are stored separately in syringes. By pushing simultaneously their plungers, they flow together in the mixing chamber and through the optical cell to reach the stop syringe. The flow stops when the plunger of the stop syringe meets an immovable block. Recording of the aging of the reaction in the optical cell is initiated just prior to the plunger stopping, thus recording some of the "flow-period". The whole system is held under constant temperature and must be hydraulically solid, i.e. no air bubbles should be present as this leads to optical artefacts. Thus,

monitoring the absorbance changes of the reaction at an adequate wavelength along the time course gives information on the concentration changes of the reactants and their reaction velocity, i. e. rate constants of the enzymatic reaction. The mathematical correlation $\Delta A_\lambda = \Delta\varepsilon_\lambda \cdot c \cdot l$ according to Beer-Lambert, where ΔA_λ is the absorption at a certain wavelength λ and $\Delta\varepsilon_\lambda$ is the molar difference absorption coefficient at a certain wavelength λ, c is the concentration of the observed product and l, the path length of the optical cell can be applied to fit the concentration range, which are directly reported by absorbance changes, to the rate equations governing the reaction. The molar difference absorption coefficient of CDH was determined as $\Delta\varepsilon_\lambda = \varepsilon_\lambda^{product} - \varepsilon_\lambda^{reactant}$.

1.5 Catalytic mechanism of CDH

CDH is a monomeric enzyme, which is divided in a *b*-type cytochrome domain with a heme *b* as the prosthetic group and a flavodehydrogenase domain with the flavin adenine dinucleotide (FAD) as the prosthetic group. The dehydrogenase domain is responsible for the oxidative and reductive half reactions, thus plays its typical role as seen within other enzyme complexes. A two-electron oxidation at the anomeric C1 position of a saccharide, such as cellobiose, is catalyzed by the FAD prosthetic group (oxidative half reaction); the hemiacetal at this position is converted to a lactone, in the case of cellobiose yielding cellobiono-1,5-lactone. The lactone then hydrolyzes spontaneously to the carboxylic acid (cellobionic acid) (Figure 5). Subsequently, the electrons are transferred from the dehydrogenase domain to an acceptor, either directly or via the heme *b* prosthetic domain; completing the reductive half reaction.

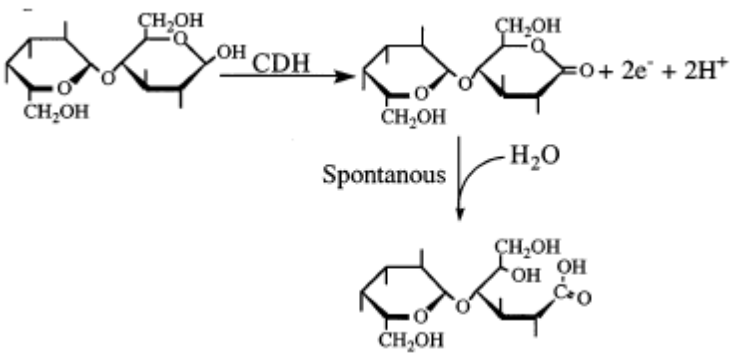

Figure 5. The oxidative half reaction of CDH. The FAD of CDH accepts two-electrons of the C1 of cellobiose to a lactone, which will spontaneously hydrolyze under ring opening to a carboxylic acid. Reference: **(15)**

Figure 7 (A) shows the schematic drawing of the redox reaction upon oxidation of cellobiose, whereas both possibilities, direct electron transfer from the dehydrogenase domain to a one or two-electron acceptor and indirect transfer via the cytochrome domain to an one-electron acceptor, are displayed. Igarashi et al. (16) determined the numbers of electrons involved in the reduction process of the two prosthetic groups. Anaerobic dithionite titration of *Pc*CDH revealed that after one-electron uptake by the heme *b*, two-electrons were distributed to the FAD until full reduction was achieved. In contrary, reduction of CDH using biological substrates so far always leads to a biphasic FAD reduction, initially, followed by a slower reduction of the heme *b*.

Two models of electron transfer as depicted in Figure 7, electron sink model and electron chain model, from the FAD to the cytochrome domain, are proposed by Henriksson et al. (15) and it is currently still under dispute under which conditions each of them can be applied. The electron sink model suggests that after one-electron from $FADH_2$ is transferred to a one-electron acceptor A, the resulting semiquinone form of FAD (FADH·) can be either further oxidized to FAD by transferring the electron to the cytochrome domain ($Fe^{3+} + e^- \rightarrow Fe^{2+}$), or can be reduced again to the fully reduced form of FAD ($FADH_2$) by the oxidation of cytochrome domain ($Fe^{2+} \rightarrow Fe^{3+} + e^-$); thus, allowing the recycled electron transfer to the one-electron acceptor A again. In the electron sink model, the electron acceptor reacts directly with the reduced FAD, which is based on the assumption that the FADH· reacts more slowly with the electron acceptor A than does the fully reduced enzyme. Electron exchange between the FAD radical and the heme *b* (electron sink) will increase the time the FAD is in the fully reduced and oxidized stages, thereby increasing the overall k_{cat}. Support of the electron sink model can also be found by the fact that all known electron acceptors, including cytochrome *c*, are reduced by the dehydrogenase domain of CDH, even if it is only present as a fragment.

Contrary, the cytochrome domain of CDH acts as an electron acceptor exclusively in the electron chain model, implying that the electron can only be transferred indirectly to the electron acceptor A via the cytochrome domain. Thus, a sequential two-step oxidation of the $FADH_2$ occurs ($FADH_2 \rightarrow FADH\cdot + e^- \rightarrow FAD + e^-$). Re-oxidation of the heme *b* prosthetic group is ensured by one-electron acceptors A in a similar manner as discussed in the electron sink model.

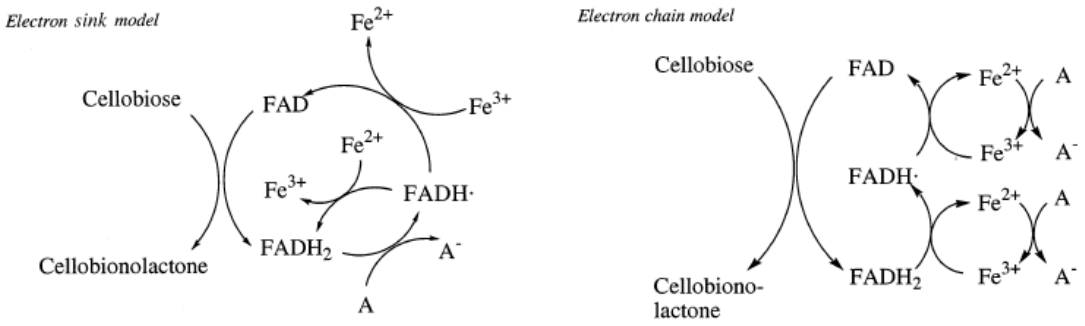

Figure 6. Mechanistic models for reduction of one-electron acceptors by CDH. Reference: **(15)**

Figure 7 (*B*) shows a schematic drawing of all rate constants involved in the oxidative and reductive half-reactions of CDH upon cellobiose oxidation and cytochrome *c* as the final electron acceptor, under the electron chain model regime. Igarashi et al. (17) in their report indicated the outraging difference between the electron transfer rate from FAD to heme *b* (30 s^{-1}) and that from heme *b* to cytochrome *c* (≈ 1500 s^{-1}). The scientists believe that this does not imply that the cytochrome domain in CDH is acting as an electron sink, which might be a misleading conclusion drawn by previous reports that the cytochrome domain is oxidized during steady-state cytochrome *c* reduction (18). Igarashi et al. (17) thus proposed that this is due to the significant difference in electron transfer rates of above mentioned reactions, and suggests that after the electron is loaded from FAD to the cytochrome domain, it is transferred to cytochrome *c* without any significant time lag, underlying the electron chain model. He highlighted the fact that his model can only be applied when cytochrome *c* is the final electron acceptor, and that redox reaction of CDH also depends and is regulated by cellobiose concentration and pH at the interdomain electron transfer step.

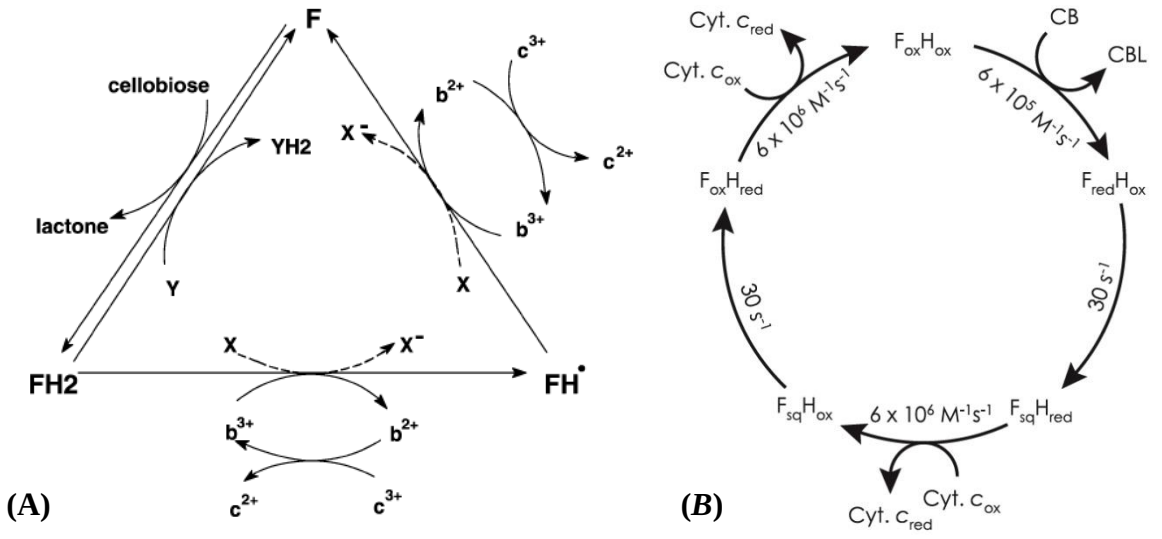

Figure 7. Mechanistic models for one- and two-electron acceptors. Reference: (A) **(19)** and (*B*) **(17)**

Depending on the models applied different reactive oxygen species are formed as different electron acceptors are involved, and yet natural electron acceptors have still to be identified. Direct electron transfer from the $FADH_2$ to molecular oxygen O_2 as a two-electron acceptor generates hydrogen peroxide H_2O_2. Indirect electron transfer from the $FADH_2$ to ferric iron (Fe^{3+}) via the cytochrome domain (electron sink model), as a one-electron acceptor and donator, yields to ferrous iron (Fe^{2+}). Fe^{3+} itself thus is a one-electron acceptor and from the biological point of view from great interest as it is abundant in wood. Eventually, Fe^{2+} and hydrogen peroxide (H_2O_2) react to form reactive hydroxyl radicals according to Fenton reaction (equation 14).

$$Fe^{2+} + H_2O_2 \rightarrow Fe^{3+} + OH^- + OH\cdot \qquad (14)$$

Several studies are consistent claiming that the biological function of CDH is to induce depolymerisation of woody substrates by generating highly reactive hydroxyl radicals via Fenton's reaction (9). Henriksson et al. (15) postulated reaction mechanisms involving the reactive hydroxyl radicals, previously produced by the transfer of the electron to the ferrous iron according to Fenton chemistry, and CDH itself, leading to the degradation of both, cellulose and lignin. Elucidating the mechanism of electron transfer in greater detail is especially from interest for cellulose and lignin degradation studies *in vivo*. It is here reminded that kinetic studies with *Mt*CDH have revealed that the pH optimum for one-electron acceptors such as cytochrome *c* is found to be 4.5 whereas for two-electron acceptors such as DCIP is found to be around 5.5 to 6.0 (20).

1.6 Crystal structure and substrate binding of CDH

Henriksson et al. (15) gives a thorough summary of substrate binding, cellulose in particular, which should be given in short here. Upon substrate binding, the enzyme is still active, thus suggesting that the substrate binding site is separate from the active site. The dissociation constant, which is defined as the concentration of unbound CDH when half of the binding sites on cellulose are occupied, is estimated to be in the sub-micromolar range and exhibit one of the lowest dissociation constants reported for cellulose binding. Cellulose binding itself is probably of hydrophobic nature and CDH binds very specific to cellulose. This is found to be evident even though one must differentiate between CDH species from basidiomycota and ascomycota, when having a closer look at the genetic footprint of CDH. In *Mt*CDH as a representative from Class-II ascomycete CDHs (21) a C-terminal carbohydrate-binding module (CBM) is highly conserved whereas the linker sequence seems to be less well conserved compared to Class-I CDH expressed by basidiomycetes who lack the C-terminal CBM. This could somewhat be related to the strong glucose discrimination in basidiomycetes which is not seen in the ascomycete *Myriococcum thermophilum*.

"True", in the sense of showing similar characteristics to the natural one, substrates for CDH are all di- or oligosaccharides with β-1,4-links and a glucose or mannose residue at the reducing end, as proposed by Henriksson et al. (15). Monosaccharides, such as glucose and mannose, and the α-1,4-diglucoside maltose exhibit very high K_M values and thus, is believed that both glucose residues bind to the active site in separate subsites. In a critical review by Henriksson et al. (15), the group report that the monosaccharides and maltose also have lower k_{cat} values indicating that binding of β-dihexosides to the active site creates an induced fit, thus stimulating catalysis, or vice versa, that monosaccharides and maltose bind to the active site in a way that is less favorable for catalysis compared to the "true" substrates. Interestingly, CDH from the ascomycete *Myriococcum thermophilum* does show very high k_{cat} values equal or even higher to those for cellobiose or lactose, while still exhibiting very high K_M values as reported by Kittl et al. (manuscript in preparation, (20)) (Table 2). The structural formulas of the substrates which had been involved in this study are depicted in Figure 8 to Figure 11 below.

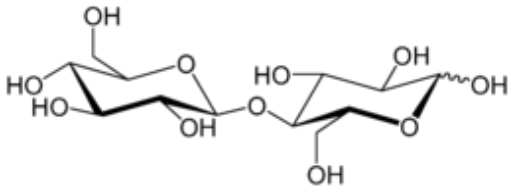

Figure 8. Structural formula of cellobiose (D-glucosyl-β-(1→4)-D-glucose)

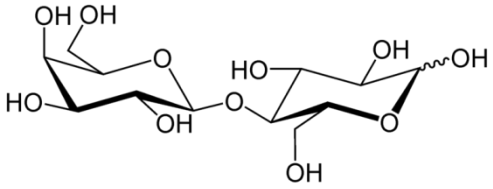

Figure 9. Structural formula of lactose (D-galactopyranosyl-β-(1→4)-D-glucose)

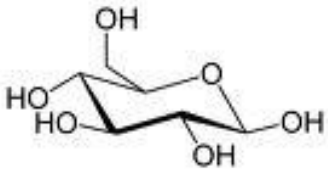

Figure 10. Structural formula of D-glucose

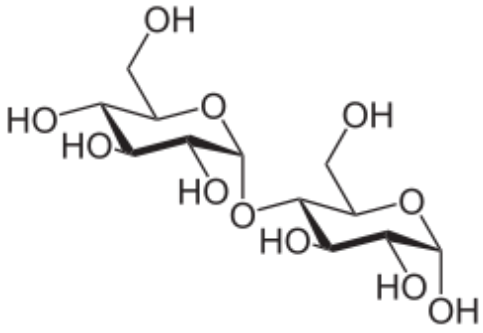

Figure 11. Structural formula of maltose (D-glucopyranosyl-α-(1→4)-D-glucopyranose)

Major focus of CDH research was on basidiomycetes, and here particularly on *Phanerochaete chrysosporium*. The theoretical crystal structure of CDH from *Phanerochaete chrysosporium* is shown in Figure 12.

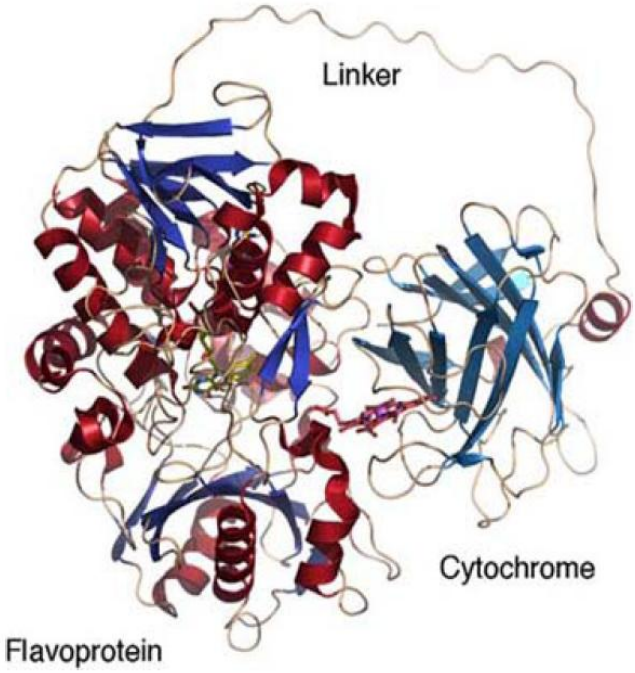

Figure 12. Theoretical *in silico* model of full-length *Pc*CDH. The N-terminal cytochrome domain and the C-terminal flavodehydrogenase domain are connected by the linker peptide. Reference: **(11)**.

Hallberg et al. (10) suggested that the cytochrome domain is complementary to the active-site entrance in the flavodehydrogenase domain and that the resulting distance between the cofactors is within acceptable limits (8 to 15 Å) for inter-domain electron transfer. Crystal structure of *Pc*CDH also revealed that the substrate cellobiose docks into the active site of the flavodehydrogenase domain; thus, Hallberg et al. proposed the enzyme discriminates against glucose by favoring interaction with the non-reducing end of cellobiose. In more detail, the crystal structure studies of *Pc*CDH (Figure 13) elaborated by Hallberg et al. in 2000 (9) and 2002 (10), suggest that there are two binding sites, subsite *C* and subsite *B*, for cellobiose on the flavodehydrogenase domain. Subsite *C* binds to the reducing end of cellobiose and is the site where catalysis takes place, whereas subsite *B* binds to the non-reducing end of cellobiose.

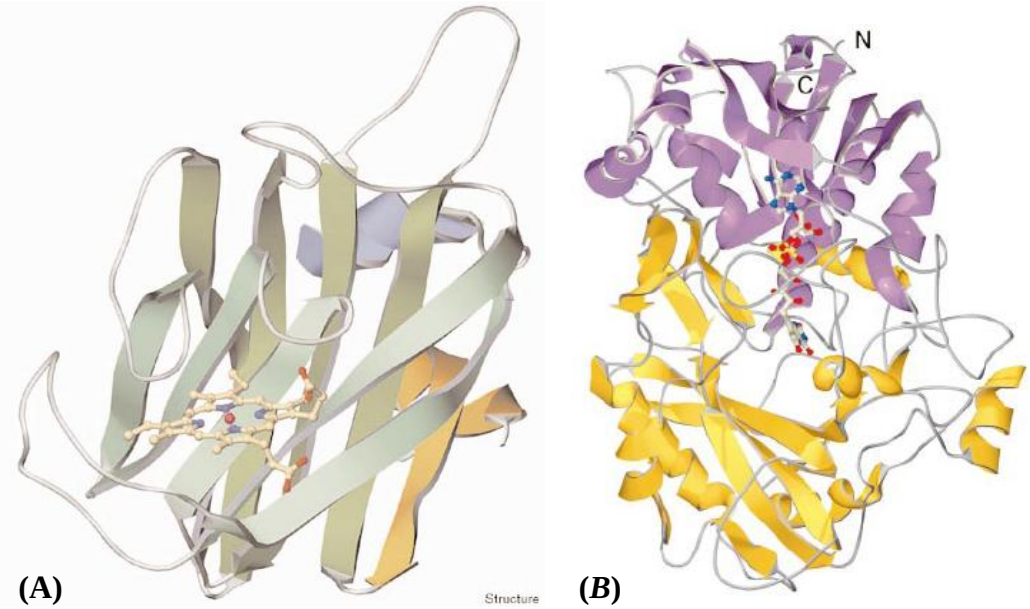

Figure 13. Structure of the separated domains of *Pc*CDH. (A) Cytochrome *b* domain. **(*B*)** Flavodehydrogenase domain. Reference: (A) **(9)** (*B*) **(10)**

However, kinetic studies have elucidated that CDH from the ascomycete *Myriococcum thermophilum* shows little glucose discrimination. The Michaelis constant (K_M) of glucose is still high; thus, glucose as the natural substrate can be ruled out as it shows low affinity to the substrate. More interestingly, as soon as this obstacle is overcome and the substrate is attached to the active site, very high rate constants (k_{cat}) are obtained. Table 2 lists the kinetic constants of *Mt*CDH (20).

1.7 Absorption spectrum of *Mt*CDH

Purified CDH exhibits a typical absorption spectrum. A major peak at 421 nm can be attributed to the heme *b* cofactor whereas the broad shoulder between 450 nm and 500 nm reflects the flavodehydrogenase domain. Zámocký et al. (11) reports that a recorded spectrum of the separated flavodehydrogenase domain showed rather small maxima at 457 nm and 496 nm. Upon reduction of CDH strong peaks appear at 429, 533 and 564 nm representing the γ (Soret), β and α band, respectively; a typical spectrum for heme *b* proteins. On the other hand, the absorption between 450 nm and 500 nm decreases, the shoulder of the flavodehydrogenase domain is thus flattened, which constitutes the reduction of the flavodehydrogenase domain.

1.8 Previous works on kinetic steady-state studies of *Mt*CDH

Here, the research was focused on CDH from *Myriococcum thermophilum* (*Mt*CDH), belonging to the ascomycota phylum. Cloning, sequence analysis and heterologous expression in *Pichia pastoris* of *Mt*CDH (CBS 208.89) was done by Zámocký et al. (21), while Kittl et al. (manuscript in preparation, (20)) did in depth analysis of kinetic constants using different electron donors and acceptors. Isolation of the *Mt*CDH gave an entire coding sequence, containing 6 introns, of 2904 bp (GenBank Accession No. EF492051), and by fusion PCR the separate amplified cDNA sequences resulted in a cDNA clone of 2487bp (GenBank Accession No. EF492052) (21). Even though kinetic steady-state studies on recombinant *Mt*CDH are not subject of this work, it was found noteworthy to include a list of the constants of steady state kinetics (Table 2) established by Kittl et al. (manuscript in preparation, (20)).

Table 2. Steady state kinetic constants of MtCDH selected electron donors and acceptors. Lactose was used for measurements of electron acceptors. All measurements were taken at 30°C, pH 4.5 if not noted otherwise. Reference: **(20)**.

electron donor	**electron acceptor**	K_m (µM)	K_I (µM)	k_{cat} (s^{-1})	k_{cat} / K_m (mM^{-1} s^{-1})
cellobiose	DCIP	**46**	3.60E+05	**12.8**	278
	cyt *c*	**3.9**	1.50E+04	**4.0**	1026
lactose	DCIP	95	9.55E+05	**12.6**	133
	cyt *c*	17.4	3.40E+04	**4.0**	227
glucose	DCIP, pH 6.0	6.80E+05	7.20E+05	**19.4**	0.029
	cyt *c*	1.44E+05	3.33E+06	**4.6**	0.032
maltose	DCIP, pH 6.0	7550	7.85E+05	1.7	0.224
	cyt *c*	4740	2.04E+06	0.8	0.165
electron acceptor	**electron donor**				
DCIP	lactose	1.2	300	16.2	1.35.E+04
	lactose, pH 6.0	7.3		16.8	2301
	lactose, pH 7.0	21		10.0	476
cyt *c*	lactose	1.2	200	9.7	8083

1.9 Previous work on *Mt*CDH surface-charge variants

Schenkenfelder (22) characterized mutants of *Mt*CDH which were designed in order to increase the intramolecular electron transfer, thus meaning the electron transfer from the FAD to the heme *b* prosthetic group. The strategy followed an exchange of negatively charged amino acid on the dehydrogenase domain to positively charged amino acids in order to reduce repulsive electric forces at neutral pH (Table 3).

Table 3. Characteristics of amino acids which were exchanged on flavodehydrogenase domain. (Reference: **(22)**)

replaced amino acid	**1-letter code**	**Polarity**	**Charge at pH 7.4**
aspartic acid	D	Polar	Negative
glutamic acid	E	Polar	Negative
exchanged amino acid	**1-letter code**	**Polarity**	**Charge at pH 7.4**
Lysine	K	Polar	Positive

The mutants under investigation in this work were produced by Schenkenfelder (22). Table 4 shows the four mutant enzymes and their used acronyms in this work, as well as protein content and molarity of the enzymes.

Table 4. Variants investigated on pre steady-state kinetics.

Variant	**acronym**	**protein content (mg/mL)**	**M (µM)**
D547K	1D	11.61	230
E550K	1E	20.59	360
D547K/E550K	2	17.4	540
D547K/E550K/E603K	3	26.2	290
D297K/D547K/E550K/E603K	4	15.68	310

Schenkenfelder (22) reports that variant D547K/E550K/E603K shows a 44-fold and 10-fold increase of cyt *c* and DCIP activity at pH 7.5, when compared to the recombinant wild-type *Mt*CDH. The quadruple mutated variant D297K/D547K/E550K/E603K showed an even higher increase in cyt *c* and DCIP activity (51-fold and 12-fold, respectively). Both of these two very promising variants, thus exhibit a ratio of DCIP/cyt *c*, which describes the intramolecular electron transfer of 2.8 compared to 9.8 for the wild-type enzyme.

2 Materials and Methods

2.1.1 Organisms

The fungus *Myriococcum thermophilum* CBS 208.89 was obtained from the Centraalbureau voor Schimmelcultures (Utrecht, Netherlands) and was maintained on PHC medium (0.5% meat peptone, 0.5% yeast extract, 0.1% magnesium sulfate, 2% α-cellulose, pH 5.4). The Pichia Easy Select Expression System with *Pichia pastoris* X-33 was obtained from Invitrogen (Carlsbad, CA, USA). Purified CDH from *Phanerochaete chrysosporium* recombinant expressed in *Pichia pastoris*, was obtained from the working group of Lo Gorton of the Department of Analytical Chemistry of the Lund University (Lund, Sweden).

2.1.2 Chemicals and media components

All chemicals and media components used were purchased in the highest grade of purity available from: Fluka (Buchs, Switzerland), Roth (Graz, Austria), Sigma Aldrich (Steinheim, Germany) and VWR (Darmstadt, Germany). Substrates for kinetic studies such as lactose, maltose and glucose and the electron acceptors: 2,6-dichloroindophenol (DCIP) and cytochrome *c* (cyt *c*, from equine heart) were obtained from Sigma Aldrich. The Bradford dye-binding assay was obtained from Bio-Rad (Hercules, CA, USA).

2.1.3 Cultivation media and solutions

All chemicals were dissolved in deionized water and autoclaved for 20 minutes at 121°C. Carbohydrates such as glucose were added only after autoclaving to avoid Maillard reaction.

2.1.3.1 YPD media

casein peptone	20 g/L
yeast extract	10 g/L
glucose	0.4% (v/v)

2.1.3.2 Fermentation basal salts medium

phosphoric acid, 85%	26.7 mL/L
calcium sulfate	0.93 g/L
potassium sulfate	18.2 g/L
magnesium sulfate·$7H_2O$	14.9 g/L
potassium hydroxide	4.13 g/L
glycerol	40.0 g/L

2.1.3.3 Trace element solution

boric acid	3.0 g/L
zinc sulfate·$7H_2O$	1.0 g/L
manganese chloride·$4H_2O$	0.3 g/L
cobalt chloride·$6H_2O$	2.0 g/L
cupric sulfate·$5H_2O$	0.1 g/L
nickel chloride·$6H_2O$	0.2 g/L
sulfuric acid conc.	4 mL/L

2.1.4 Buffer systems

The buffers were prepared with deionized water, sterile-filtrated and degassed before use. For chromatography purposes, buffers for equilibration and elution are denoted by “Buffer A” and “Buffer *B*”, respectively.

2.1.4.1 PHE-Reference (HIC)

Buffer A

50 mM NaAc, pH 5.0

0.3 M NaCl

20% saturation $(NH_4)_2SO_4$

Buffer B

50 mM NaAc, pH 5.0

2.1.4.2 Q Reference (AEC)

Buffer A

50 mM NaAc; pH 5.5

Buffer B

50 mM NaAc; pH 5.5

1 M NaCl

2.1.4.3 Mono Q Reference (AEC)

Buffer A

20 mM Tris-HCl, pH 8.0

Buffer B

20 mM Tris-HCl, pH 8.0

1 M NaCl

2.1.4.4 Activation buffer (papain)

100 mM $NaPO_4$, pH 7.0

2 mM EDTA

2 mM DDT

2.1.5 Heterologous protein expression

The encoding cDNA for CDH originated from the fungus *Myriococcum thermophilum* CBS 208.89 which was obtained from Centraalbureau voor Schimmelcultures (Utrecht, Netherlands). The cDNA was ligated into the expression vector pPICZαB and transformed into competent *Pichia pastoris* X-33 cells by electroporation. Transformants were selected on YPD plates containing 1000 µg/L Zeocin. Isolation, cloning and heterologous expression in *Pichia pastoris* on small scale was not performed within the scope of this work; thus, for further details consult (21). Growth of the pre-culture was performed in two baffled flasks each containing 200 mL YPD medium at 30°C under intense shaking overnight, until OD_{600} reached the value of 2.8. The overnight pre-culture of *Pichia pastoris* transformant of 400 mL volume, was then inoculated into a 4 L production stage medium in a 7 L MBR fermenter (MBR Bioreactor, Wetzikon, Switzerland). The fermentation was performed according to the manual of the *Pichia* fermentation process guidelines (Invitrogen, Version *B*, 053002) (23), a 3-step production process (glycerol batch phase, glycerol fed-batch phase and methanol fed-batch phase) with monitoring and regulation of agitation to 600 rpm, temperature to 30°C, pH to 5.5, dissolved oxygen and feed. Antifoam was added initially and during the fermentation as needed. Sampling (10 mL) was performed at least twice daily, monitoring cell growth by determining OD_{600} and wet cell weight as soon as the methanol feed started. After initiating enzyme production, the extracellular protein content and enzyme activity using DCIP and cytochrome *c* as electron acceptors was measured in the supernatant of the samples. After adjusting the pH to 5.0 with ammonia, an initial addition of 4% (v/v) glycerol and 0.4% (v/v) PTM_1 Trace Salts under aseptic conditions, the glycerol batch phase was started, keeping the pH at 5.5 and the dissolved oxygen above 20%. After 22 hours, glycerol feed was started in order to increase the cell biomass under limiting conditions, with an average addition of 18 mL per hour and initial fermentation volume. 1.2% (v/v) PTM_1 Trace Salts was added under aseptic conditions to the glycerol feed. After two hours, the transition phase to methanol was started by adding 0.15% (v/v) of methanol to fermentation broth, while at the same time the glycerol feed was decreased gradually over three hours until the cells were fully adopted to methanol with an increasing feed rate from 7 to 10 mL/h and initial fermentation volume; 1.2% (v/v) PTM_1 Trace Salts to methanol feed was given manually under aseptic conditions. Under these conditions, fermentation continued over 130 hours until late stationary phase. The fermentation broth (6.75 L) was harvested and centrifuged (RC26-PLUS, Rotor SLA-3000) for 15 min at 4000 rpm at 4°C, yielding to supernatant volume

of 2935 mL. The supernatant was stabilized with 20% (v/v) ammonium sulfate before starting the purification procedure.

2.1.6 Enzyme purification

The enzyme was purified by using hydrophobic interaction chromatography (HIC), followed by a strong anionexchange chromatography (AEC) step. Aliquots of supernatant were applied to a 420 mL PHE Sepharose fast flow column (XK 50/30 (GE Healthcare, Waukesha, WI, USA), pre-equilibrated with 50 mM sodium acetate buffer, pH 5.0 containing 0.3 M sodium chloride and 20% (v/v) saturated ammonium sulfate. The proteins were eluted with a linear gradient to 50 mM sodium acetate buffer, pH 5.0, in 10 column volumes (CV). Fractions were tested for CDH activity and protein content, and those with high specific CDH activity were pooled and diafiltrated (Amicon Ultra-15 Centrifugal Filter Units, Ultracel 10 membrane, 10 kDa) against 50 mM sodium acetate buffer, pH 5.5, to a conductivity below 5 mS/cm. The pool was applied on an AEC fast flow Q Reference column (21 mL), pre-equilibrated in the same buffer as the protein pool. Elution was performed with a linear salt gradient from 0 to 1 M sodium chloride in 15 CV. Fractions with significant absorption at both 420 nm and 450 nm were tested for CDH activity and protein content; those with high specific CDH activity were pooled. A third purification step was performed due to instability problems using an AEC fast flow Q Reference consistent with the previous one with the only exemption that elution was performed with 20 CV in order to get a higher separation resolution. The separation principle is based on different pI of the proteins to be separated. In AEC, resin residues are positively charged and the protein to be separated must have a negative net charge. Thus, the pH of its surrounding must be higher than the pI of the protein, resulting in a negative net charge of the protein. As the flavodehydrogenase domain, CDH and cytochrome domain exhibit a pI of approximately 5.5, 4.0 and 3.5, respectively (11), the flavodehydrogenase domain should not bind to the resin as total net charge should be neutral or slightly positive and flow through, whereas CDH comes next with the elution buffer, and the cytochrome domain should bind strongly and should be eluted only at the a high gradient of buffer *B*, i.e. high chloride concentration replacing negatively net charged cytochrome domain. Testing the fractions for CDH activity and protein content, those with similar characteristics were pooled, ultrafiltrated (Sorvall Evolution RC Centrifuge; Amicon Millipore, 10 kDa; 4 x 3500 rpm à 20 min) and re-buffered in 20 mM sodium acetate, pH 5.5 and 100 mM sodium acetate, pH 5 for the two CDH pools and flavodehydrogenase domain pool,

respectively, sterile-filtrated and stored at - 80°C for longer periods and 4°C for usage within 3 weeks.

2.1.7 Protein characterization

UV-Vis spectra of purified recombinant *Mt*CDH were recorded by a Hitachi U-3000 split-beam spectrophotometer in the range of 200 nm to 600 nm at room temperature. Spectra of CDH in the oxidized and reduced state were recorded for recombinant *Mt*CDH, *Pc*CDH and deglycosylated *Pc*CDH. Reduction was performed catalytically or chemically by adding 300 mM lactose or sodium dithionite. Absorption coefficients employed for photometric measurements for determination of protein content of *Mt*CDH were obtained as followed; for the holoenzyme CDH ε_{280} = 159.063 $mM^{-1}cm^{-1}$, FAD ε_{280} = 112.738 $mM^{-1}cm^{-1}$ and heme *b* ε_{280} = 46.263 $mM^{-1}cm^{-1}$.

Sodium dodecyl sulfate – polyacrylamid gel electrophoresis (SDS-PAGE) was carried out with an Amersham-Pharmacia Phast System (GE Healthcare) using precast PhastGel gradient gels (8-25%). Proteins were visualized with Coomassie Brilliant Blue.

Protein content was determined using the assay according to Bradford (24). CDH activity was determined using lactose as electron donor and both, the two-electron acceptor 2,6-dichloroindophenol (DCIP) and the one-electron acceptor cytochrome *c* (cyt *c*). By transfer of two-electrons from the flavodehydrogenase domain to DCIP, the decolorization of the initially red-blue assay can be easily detected. The reduction of DCIP thus, is proportional to the decrease in absorption at 520 nm in a pH lower than 6, with an absorption coefficient ε_{520} of 6.9 $mM^{-1}cm^{-1}$. Cyt *c* on the other hand, is a one-electron acceptor and exclusively gets its electron from the cytochrome domain of the enzyme. Hence, only active CDH as a holoenzyme is detected with this assay as the cytochrome domain is not catalytically active by its own (19). The increase of absorption, where the initially orange color of cyt *c* changes to a more reddish tone, is proportional to the reduction of cyt *c* at 550 nm, with an absorption coefficient ε_{550} of 21.2 $mM^{-1}cm^{-1}$. These standard enzyme assays are modifications of (25). One Unit of enzyme activity is defined as the amount of enzyme that reduces 1 µmol of substrate, i.e. e. DCIP or cyt *c* per minute under the selected assay conditions. In this work, all data concerning enzyme activity of steady-state measurements are defined as such. All solutions for assays and SDS-PAGE were prepared and conducted according to the manuals provided by the working group of the Food Biotechnology Laboratory (H75 Department of Food Sciences and Technology).

2.1.8 Deglycosylation and partial proteolytic digestion experiments

Deglycosylation of purified recombinant *Mt*CDH on a small scale was performed using Endoglycosidase Hf (EndoHf; 10 µL/mg CDH), which cleaves within the chitobiose core of high mannose and hybrid oligosaccharides from N-linked glycoproteins, and α-mannosidase (0.1 mg/mg CDH) in order to facilitate EndoHf entry to its cleaving sites. The reaction mixture was incubated at 37°C over night and analyzed on SDS-PAGE gels.

Partial proteolytic digestion was performed on a small scale in order to cleave both, glycosylated and deglycosylated *Mt*CDH at the linker region to yield single flavodehydrogenase and cytochrome domains. Papain was used for proteolytic digestion; 10 mg/mL papain was incubated at 25°C for 60 min with activation buffer in the ratio 1:5. Then, four volume parts of CDH with a concentration of 15 mg/mL and one volume unit of 1 M sodium acetate buffer, pH 5, was added to one volume unit of the activated papain solution and incubated for 60 min at 25°C. In order to stop the digestion, the mixture was quickly loaded on an AEC fast flow Q Reference column (1 mL), pre-equilibrated in 20 mM Tris-HCl, pH 8; after desalting and re-buffering of the mixture. Elution was performed with a linear gradient from 0 to 1 M sodium chloride in 50 CV. Deglycosylation and partial proteolytic digestion trials were not successful in respect to this work; hence, results are not from further interest of discussion.

2.1.9 Reconstitution of the FAD

Reconstitution trials of the flavodehydrogenase domain were conducted to evaluate if all flavodehydrogenase domains of the purified *Mt*CDH were fully occupied by the cofactor FAD. One volume unit of FAD-deficient *Mt*CDH was mixed with 1.2 volume units of a stock solution (10 mg/mL) of FAD, diluted 1:5 with 50 mM sodium phosphate buffer, pH 4.0, and incubated over night at room temperature. Unbound FAD was washed out by ultracentrifugation against 50 mM sodium phosphate buffer, pH 6.0, until no FAD was detected at 450 nm in the flow through.

2.1.10 Pre steady-state experiments

The rapid spectral change of CDH upon mixing with various substrates was recorded using a SX20 Photophysics Stopped-Flow Spectrometer (Leatherhead, UK) with a 1 cm observation path length at 30°C in 100 mM buffers (citrate phosphate and sodium acetate for measurements with *Mt*CDH and *Pc*CDH, respectively). The reaction chamber had a volume of 20 µL and the

two reaction species were mixed in a 1:1 ratio (10 µL each). The spectra were recorded in the photodiode array mode within the range of 182 to 725 nm.

Determination of the dead-time of the instrument was done according to Palfey (26). Final enzyme concentration was determined to be 5 µM. Pre steady-state kinetics measurements with recombinant wild-type *Mt*CDH were performed with various substrates with different concentrations, i.e. cellobiose, lactose, glucose, mannose, as well as with lactose (50, 500, 50000 µM) at different pH values, in the range of 3.0 to 7.5. Recombinant *Mt*CDH surface-charge variants (D547K, E550K, D547K/E550K, D547K/E550K/E603K and D297K/D547K/E550K/E603K) were measured against lactose (50 and 500 µM) and glucose (5 and 50 mM) at pH 4.5 and 7.5. Recombinant wild-type *Pc*CDH and an aliquot which was deglycosylated (final concentrations both 5 µM) were measured against 50 mM lactose at pH 4.5. Data analysis was accomplished with Pro-Data SX software package.

Reduction of the FAD and heme *b* prosthetic groups can be directly monitored at 449 and 562 nm, respectively. In order to determine the reduction rates of the prosthetic groups in CDH, the absorption difference between 510 (oxidized) and 483 (reduced) for the FAD and absorption difference between 572 (oxidized) and 562 (reduced) for the heme *b* were calculated (27). As the reduction of the FAD showed biphasic behavior it was fitted to a double exponential curve until it reached equilibrium. Contrary, the reduction curve for heme *b* showed an initial lag phase with monophasic behavior; thus, a single exponential fitting was applied. Molar difference absorption coefficients (reduced minus oxidized state of prosthetic group) employed were for heme *b* $\Delta\varepsilon_{562\text{-}572}$ = 24.0 mM^{-1} cm^{-1} and FAD $\Delta\varepsilon_{483\text{-}510}$ = 6.3 mM^{-1} cm^{-1}, respectively.

The pre steady-state kinetic constants, i.e. limiting rate constant k_{lim}, dissociation constant K_d and substrate inhibition constant K_i, were determined according to Igarashi et al. (16). For FAD reduction, he suggested to fit the hyperbolic substrate concentration dependence to the equation 15.

$$k_{obs} = k_{lim} \cdot S / (K_d + S) \qquad (15)$$

In order to determine the k_{lim} of the much slower phase (second phase of FAD reduction and for the heme *b* reduction), equation 16 was used from a former substrate inhibition study of flavocytochrome b_2 by Rouvière et al. (28) where uncompetitive substrate inhibition is assumed.

$$k_{obs} = k_{lim} \cdot S / (K_d + S + S^2/K_i) \qquad (16)$$

Moreover, the assumption is made that after reduction upon carbohydrate oxidation no re-oxidation of the enzyme occurs.

3 Results and Discussion

3.1 Fermentation and purification of recombinant *Mt*CDH

Heterologous production of *Mt*CDH in *Pichia pastoris* was performed as described in 2.1.5. Wet cell weight, enzyme activity and protein content after first induction of methanol until harvesting are summarized and depictured in (Table 5 and Figure 14). The specific activity in the fermentation broth after 132 hours was 1.38 U/mg and 0.14 U/mg for DCIP and cyt *c*, respectively. Thus a DCIP/cyt *c* ratio of 20:1 was achieved, indicating a high abundancy of the flavodehydrogenase domain in the crude extract.

Table 6 shows a comprehensive list of purification parameters for evaluation of both, fermentation and purification. Table 7 shows the purification scheme of *Mt*CDH. After centrifugation, the supernatant consisted of proteins, amongst others CDH, and other impurities still soluble, such as cell and media components. The supernatant (2935 mL) was high in total protein of 3161 mg, and showed modest specific activities of CDH (1.82 U/mg and 0.24 U/mg when using DCIP and cyt *c* as electron acceptors). The HIC purification step resulted in a 1.3-fold purification compared to the supernatant, for both activity assays. The flavodehydrogenase domain was still present after HIC purification as two major bands at approximately 85 and 100 kDa for the flavodehydrogenase domain and CDH holoenzyme, respectively, can be seen on the gel (Figure 15, (A)). The flavodehydrogenase domain is more prominent after HIC than before, compared to CDH holoenzyme content. Interestingly, electrophorestic analysis also shows after HIC was performed, a vague band at approximately 35 kDa, which could be evidence for the cytochrome domain. Therefore, it can be assumed that CDH is instable in the elution buffer of HIC. After the first AEC chromatography, hardly any purification was obtained compared to high protein leakage. As SDS-PAGE still showed flavodehydrogenase domain impurities, an additional purification step was thus necessary. Thus, a second AEC chromatography step was applied, yielding a 1.4-fold and 4.8-fold purification, compared to crude extract, for DCIP and cyt *c* assay, respectively. Protein loss was very high, with only 5.1% and 13.05% highly purified CDH from the starting activity, for DCIP and cyt *c*, respectively, compared to crude extract. The fractions which showed similar CDH activities were pooled, yielding to two enzyme solutions with different grades of purity. r*Mt*CDH1 showed higher specific activity of DCIP relatively to cyt *c* than r*Mt*CDH2; thus, leading to a ratio of 3.5 and 2.2 units of DCIP to one unit cyt *c* for

r*Mt*CDH1 and r*Mt*CDH2, respectively. SDS-PAGE revealed that the fractions were free of the flavodehydrogenase domain, with bands of approximately 100 kDa present (CDH holoenzyme) (Figure 15, (C)). Both fractions of highly purified CDH were re-buffered with 20 mM sodium acetate, pH 5.5, steril-filtrated and aliquots stored at 4°C and – 80°C. r*Mt*CDH1 showed a spectral ratio of A_{420}/A_{280} of 0.64 and was satisfactory for usage on further experiments.

It seems that a major part of the CDH had been partially digested either during fermentation by *Pichia pastoris* produced proteases or had been degraded along the purification process, as the two separated protein fractions show a high content in the flavodehydrogenase domain. Evidence for partial digestion by proteases could be the increasing protein content while DCIP activity is already falling in the end period of fermentation (Figure 14). The protein content of the separated flavodehydrogenase domain constitutes 20% of all proteins in the crude extract supernatant, whereas the highly purified CDH can be only attributed for 6% of total protein in crude extract supernatant. Thus, catalytically active flavodehydrogenase domain was separated from CDH after the first AEC chromatography and re-buffered in 100 mM sodium acetate, pH 5.0. The flavodehydrogenase domain fraction was encoded as r*Mt*CDH5 and shows a specific activity of 5.85 U/mg. Electrophoretic analysis proved that the flavodehydrogenase domain with a molecular weight of 75 kDa had been separated from CDH holoenzyme and is without any impurities (Figure 15).

Zámocký et al. (21) also reported that recombinant production in a fermenter using a mineral medium had yielded predominantly the *Mt*CDH flavodehydrogenase domain, while intact CDH is rare. This is confirmed by this work, as yields are low and FAD constitute 77% of total activity compared to only 12% by CDH, both measured with DCIP as electron acceptor and where 100% is determined as total activity after HIC (Table 6).

Table 5. Cell growth and enzyme activity during fermentation. Shown are parameters before methanol feed was started (0) until end point of fermentation.

time (h)	wet cell weight (mg/L)	DCIP (U/mL)	cyt *c* (U/mL)	protein (mg/mL)
0	139.3	0.00	0.00	
24	223.4	0.14	0.03	
48	291.5	0.84	0.06	
72	315.0	1.61	0.15	
96	311.5	1.62	0.19	0.82
120	310.0	2.59	0.26	0.78
132	331.5	2.11	0.21	1.53

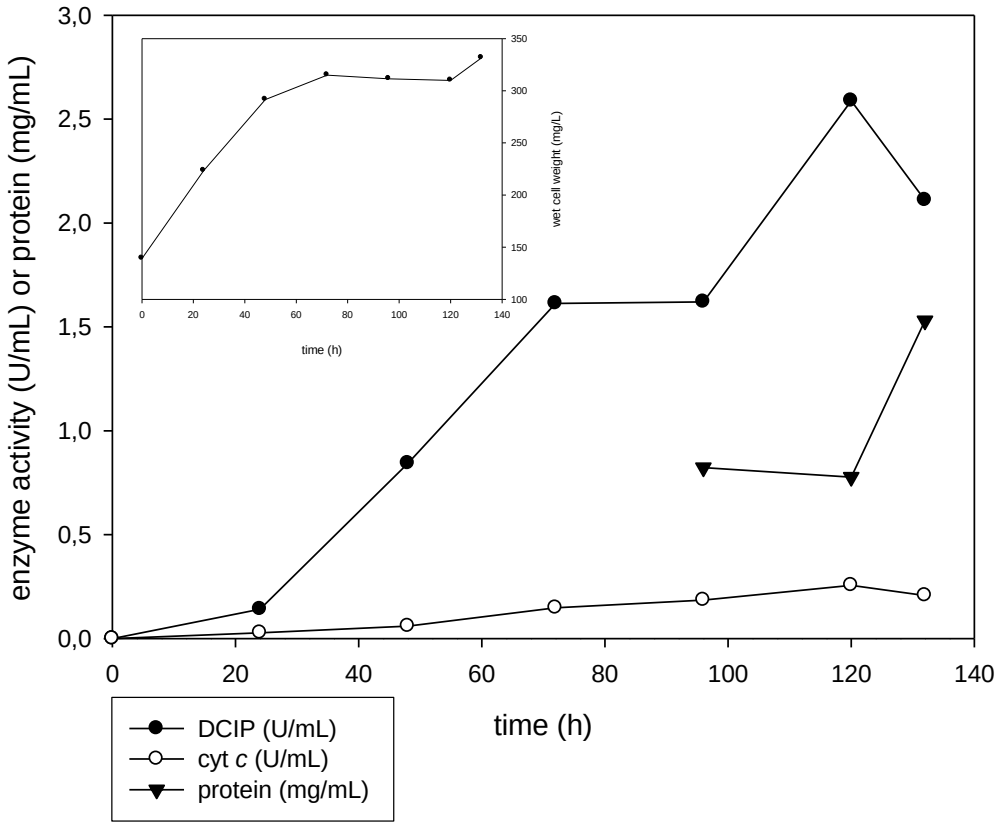

Figure 14. Cell growth and enzyme activity during fermentation. Shown are parameters beginning with methanol induction at (0) unti end point of fermentation.

Table 6. Purification scheme of recombinant *Mt*CDH.

purification stage	Fractions	code	volume (mL)	total protein (mg)	total activity (U)[1]	total activity (U)[2]	specific activity (U/mg)[1]	specific activity (U/mg)[2]	DCIP : cyt c	NaAc buffer
fermentation supernatant			2935	3161	5758	736	1.82	0.23	7.82	
PHE-source (HIC)			252	2051	4798	608	2.34	0.30	7.89	
1st Q-source (AEC)	**flavodehydrogenase domain**	r*Mt*CDH5	150	633	3701	0	**5.85**	0.00	-	100 mM, pH 5.0
	CDH holoenzyme		102	835	2622	222	3.14	0.27	11.81	20 mM, pH 5.5
2nd Q-source (AEC)	**CDH holoenzyme**	r*Mt*CDH1	17.2	135	438	126	**3.24**	**0.93**	3.48	20 mM, pH 5.5
		r*Mt*CDH2	7	59	148	66	**2.51**	**1.12**	2.24	

Table 7. Determination of purification level and yield.

purification stage	Code	purification level[1]	purification level[2]	yield (%)[1]	yield (%)[2]
fermentation supernatant		1	1	100	100
PHE-source (HIC)		1.3	1.3	83.3	82.6
1st Q-source (AEC)		1.7	1.1	45.5	30.2
2nd Q-source (AEC)	r*Mt*CDH1	1.8	4.0	7.6	17.1
	r*Mt*CDH2	1.4	4.8	2.6	9.0

[1] CDH activity assay using DCIP as electron acceptor and lactose as electron donor, pH 4.5

[2] CDH activity assay using cyt *c* as electron acceptor and lactose as electron donor, pH 4.5

3.2 Enzyme characterization

3.2.1 Electrophoretic analysis

Recombinant *Myriococcum thermophilum* CDH has a molecular weight of approximately 100 kDa whereas the flavodehydrogenase domain is about 85 kDa (Figure 15, (C)). Thus, previous reports by Zámocký (21) are confirmed.

Electrophoretic analysis clearly states that after HIC the band representing the flavodehydrogenase domain on the gel is more dominant than the band representing CDH holoenzyme (Figure 15, (A)). This is consistent with the high DCIP/cyt *c* ratio shown in the purification protocol (Table 6).

Compared to recombinant CDH from *Phanerochaete chrysosporium*, *Mt*CDH is rather small as recombinant *Pc*CDH investigated here showed bands at 150 kDa and 85 kDa for CDH holoenzyme and flavodehydrogenase domain, respectively (Figure 15, (D)). Deglycosylated CDH from *Phanerochaete chrysosporium* is fairly instable as several bands are revealed by electrophoretic analysis with a dominant band at approximately 80 kDa, and three lighter ones at 130 kDa, 85 kDa and 60 kDa, presumably indication proteolytic degradation. Both, *Pc*CDH without any treatment and deglycosylated *Pc*CDH were stored at 4°C for approximately ten days until SDS-PAGE was performed.

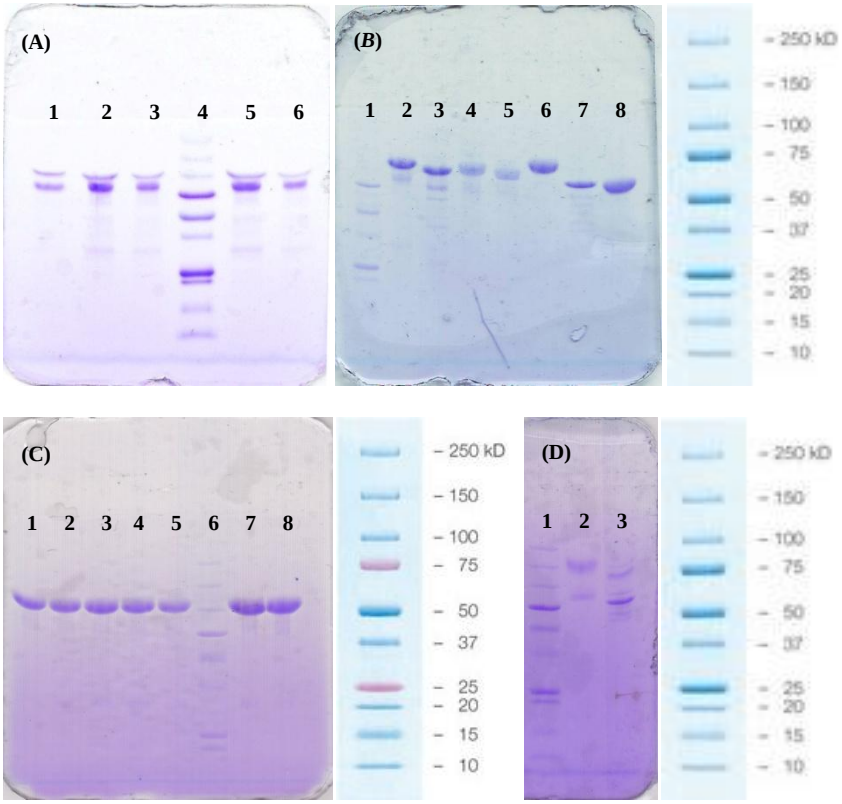

Figure 15. SDS-PAGE of recombinant *Mt*CDH and recombinant *Pc*CDH. (A) *Mt*CDH before and after HIC purification stage. 2 µg crude extract of supernatant (1), 4 µg post-HIC (2) and (5), 2 µg post-HIC (3) and (6), standard (4). **(*B*)** Separated flavodehydrogenase domain of *Mt*CDH after 1st AEC. standard (1), 0.5 µg r*Mt*CDH5 (8). **(C)** *Mt*CDH after 2nd AEC (0.5 µg of protein had been loaded). Aliquots of r*Mt*CDH1 before pooling (1)-(5), standard (6), r*Mt*CDH1 (7), r*Mt*CDH2 (8). **(D)** Electrophoretic analysis of *Pc*CDH (0.5 µg of protein had been loaded). Standard (1), *Pc*CDH not treated (2), deglycosylated *Pc*CDH (3). Standards were either Precision Plus Protein All Blue Standards or Precision Plus Protein Dual Color Standards (Bio-Rad).

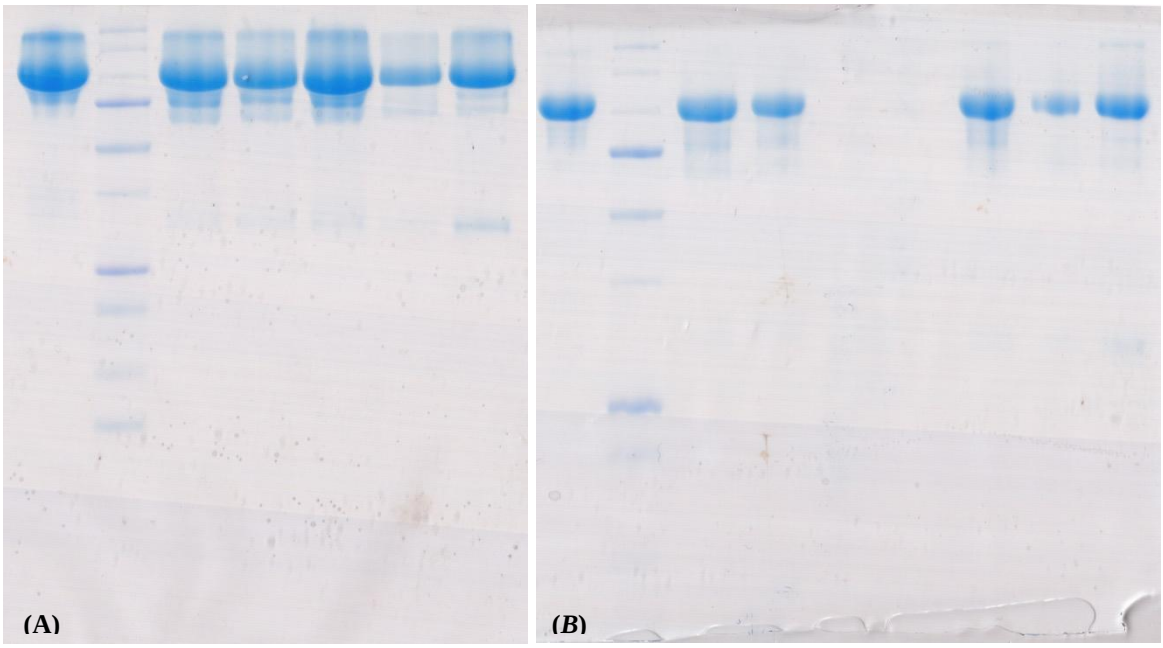

Figure 16. SDS-PAGE of recombinant *Mt*CDH wild-type and variants. (A) 2 µg loaded. wt *Mt*CDH (1), Standard (2), D547K (3), E550K (4), D547K/E550K (5), D547K/E550K/E603K (6) and D297K/D547K/E550K/E603K (7). **(*B*)** 0.5 µg loaded. wt *Mt*CDH (1), Standard (2), D547K (3), E550K (4), D547K/E550K (7), D547K/E550K/E603K (8) and D297K/D547K/E550K/E603K (9). Standard used was Precision Plus Protein All Blue Standards.

3.2.2 UV-Vis spectra

The different investigated CDHs show a typical absorption spectrum of CDH (see 1.7). Small differences between species occur, as well as within a species with different glycosylation patterns of the protein occur (Figure 17, Figure 18 and Figure 19). These differences occur in the position of the bands and the amplitude of absorption.

Addition of sodium dithionite reduced the enzyme totally, revealing that it had not been reduced completely by lactose alone. The α-band at 562 nm for *Mt*CDH showed an adsorption of 0.198 catalytical and 0.253 by chemical reduction. Thus, only 75% of the enzyme had been reduced by lactose.

The difference spectrum reveals different amplitudes of adsorption for *Pc*CDH, deglycosylated *Pc*CDH and *Mt*CDH, depicted in Figure 20.

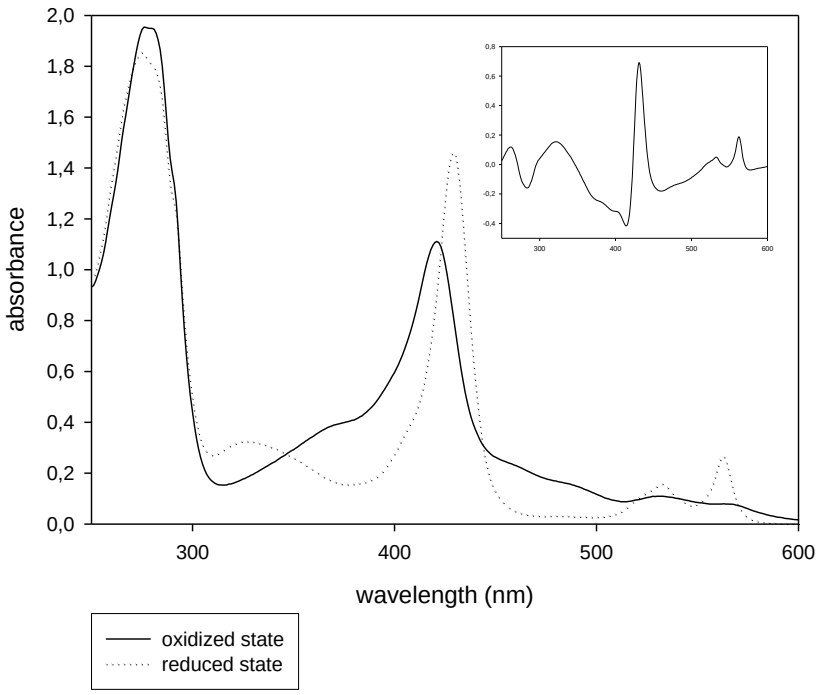

Figure 17. Oxidized and reduced UV-Vis spectrum of recombinant *Pc*CDH. Catalytic reduction was performed by adding 300 mM lactose. Small graph shows difference spectrum (reduced minus oxidized). The ratio A_{420}/A_{280} is 0.57.

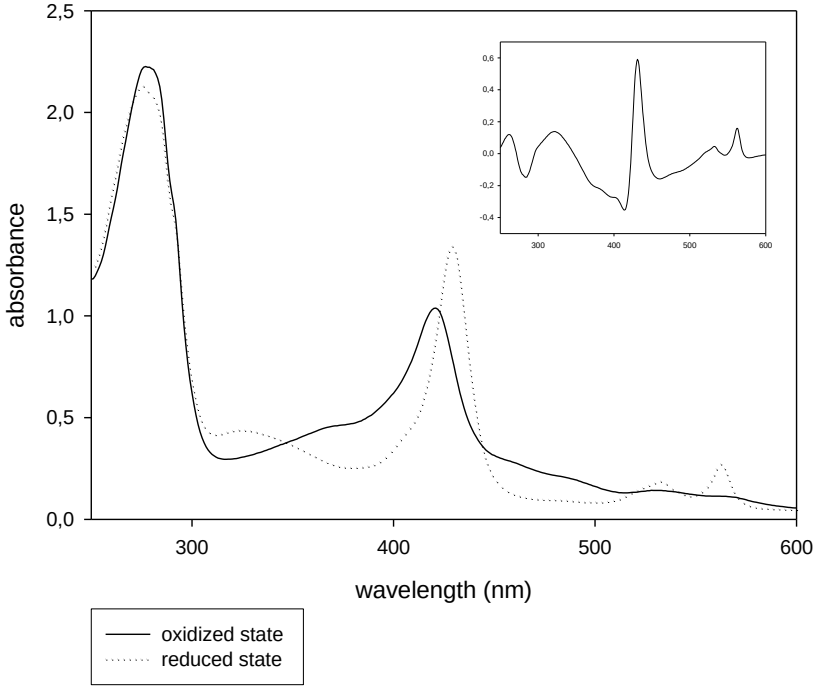

Figure 18. Oxidized and reduced UV-Vis spectrum of deglycosylated recombinant *Pc*CDH. Catalytic reduction was performed by adding 300 mM lactose. Small graph shows difference spectrum (reduced minus oxidized). The ratio A_{420}/A_{280} is 0.47.

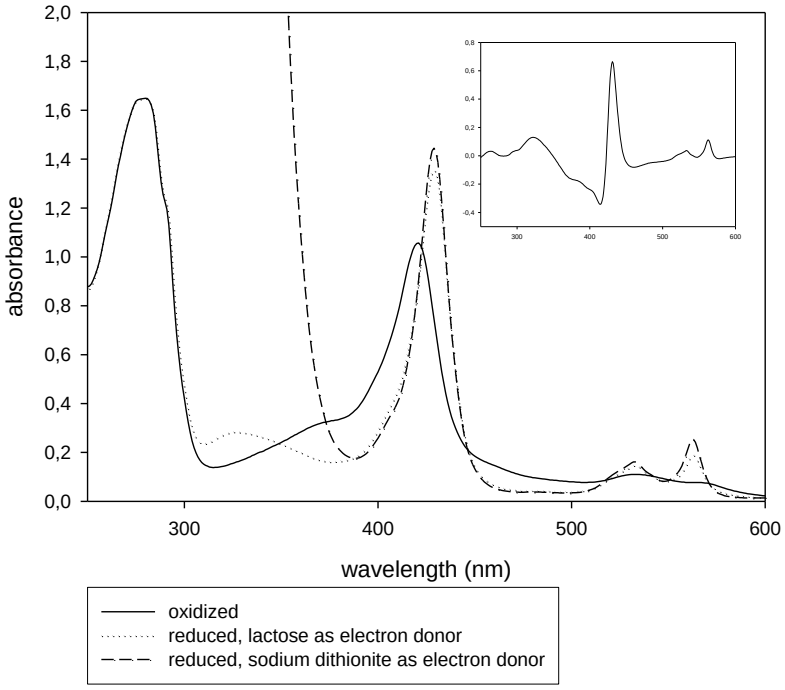

Figure 19. Oxidized and reduced UV-Vis spectrum of recombinant r*Mt*CDH1. Catalytic reduction was performed by adding 300 mM lactose. Chemical, thus, total reduction was achieved by adding sodium dithionite. Small graph shows difference spectrum (reduced minus oxidized). The ratio A_{420}/A_{280} is 0.64.

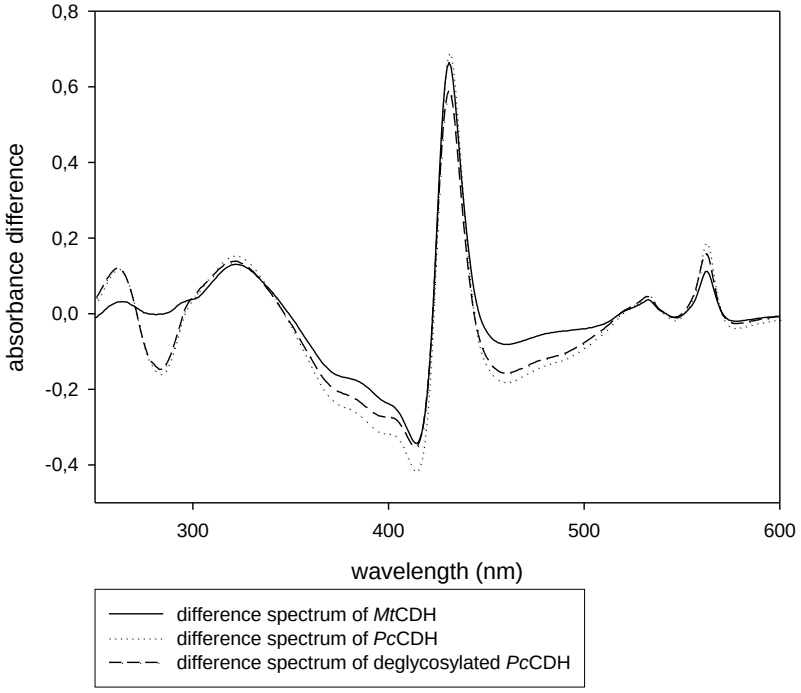

Figure 20. Comparison of difference spectra. Absorption of reduced state minus oxidized state of enzyme. Reduction by 300 mM lactose.

3.2.3 Reconstitution of flavodehydrogenase domain in recombinant *Mt*CDH

After the first AEC chromatography the enzyme had been subject to reconstitution of flavodehydrogenase domain according to procedures mentioned in 2.1.9. The results show a decrease in protein content (minus 84%) and specific activity with the DCIP assay (minus 11%), whereas a considerable increase in cyt *c* activity (plus 41%) as stated in Table 8.

This could give evidence to the fact that indeed some flavodehydrogenase domain had not been occupied by FAD cofactors. Moreover, it can be assumed that unbound FAD cofactors also compete with intact CDH, thus, lowering its enzymatic activity. This could also explain the generally low activity of recombinant *Mt*CDH reported already by (21).

Table 8. *Mt*CDH before and after reconstitution of flavodehydrogenase domain. The enzyme under investigation here was from the fractions of 1st AEC.

	protein (mg/mL)	**specific activity (U/mg)[1]**	**specific activity (U/mg)[2]**	**DCIP : cyt c**	**buffer**
*Mt*CDH	6.97	3.15	0.66	4.74	20 mM NaAc, pH 5.0
*Mt*CDH reconstituted	1.14	2.80	0.94	2.99	50 mM Na_3PO_4, pH 6.0

3.3 Pre steady-state kinetics

3.3.1 Reduction of recombinant *Mt*CDH with various substrates

The spectrum of *Mt*CDH upon mixing with cellobiose changed from the oxidized to the reduced form more slowly than previously reported with *Pc*CDH (16). Its complete reduction was obtained only after 5.8 s, with an initial lag phase of the heme *b* reduction observed at 563 nm of 0.05 s (Figure 21, Figure 22 and Figure 23).

At 449 nm FAD reduction showed a biphasic behavior; an initial fast reduction where 42% were reduced after 0.1 s was followed by a slow reduction where 69% were reduced after 1.0 s (Figure 24). Complementary, heme *b* reduction was very slow in the beginning but increased as FAD reduction slowed down. Heme *b* reduction was monitored at 563 nm showing the following reduction characteristics in time; 8.3% after 0.1 s and 60% after 1.0 s (Figure 25). Eventually, reduction of the holoenzyme CDH was completed after 5.8 s where both prosthetic groups, the FAD and cytochrome domain, reached full reduction in steady state.

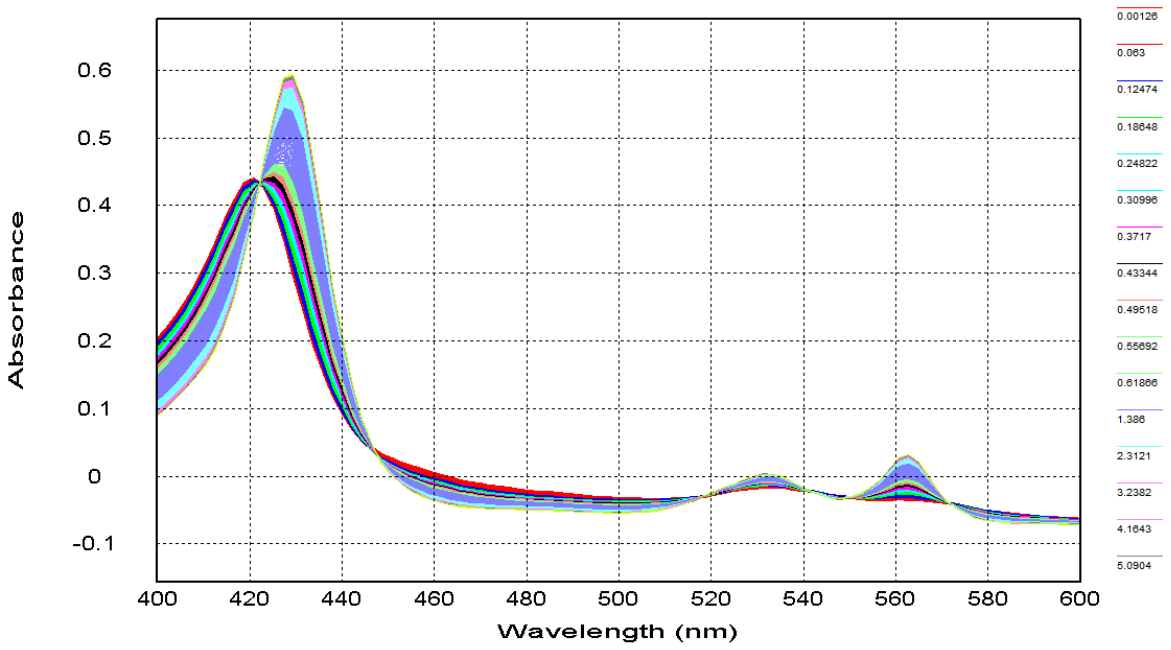

Figure 21. Pre steady-state spectral changes of *Mt*CDH upon mixing with cellobiose. CDH and cellobiose (final concentrations of 5 and 500 µM respectively) were mixed in 100 mM sodium acetate (pH 4.5) at 30°C, along the time course.

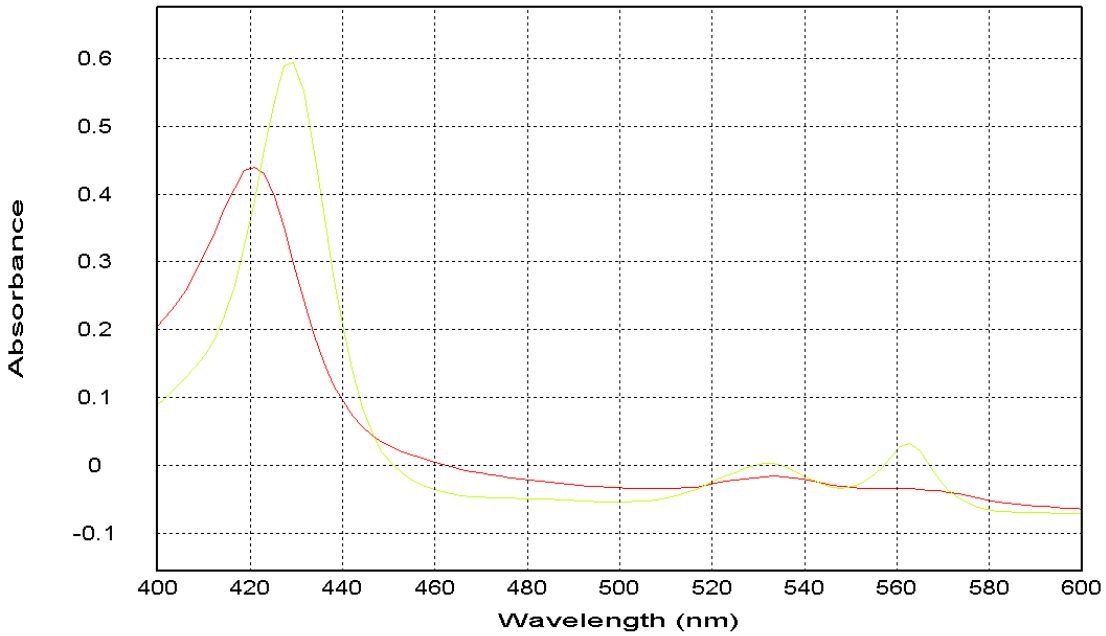

Figure 22. Pre steady-state spectral changes of *Mt*CDH upon mixing with cellobiose. Oxidized spectrum is depicted in red and reduced spectrum is depicted in green. CDH and cellobiose (final concentrations of 5 and 500 µM respectively) were mixed in 100 mM sodium acetate (pH 4.5) at 30°C.

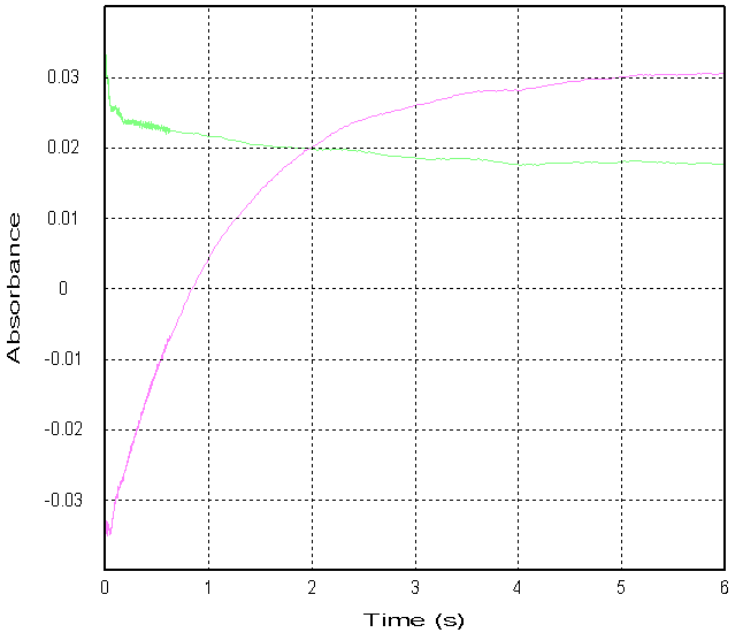

Figure 23. Pre steady-state spectral changes of *Mt*CDH at 449 nm (FAD, green line) and 562 nm (heme *b*, pink line) upon reduction of cellobiose. CDH and cellobiose (final concentrations of 5 and 500 µM respectively) were mixed in 100 mM sodium acetate (pH 4.5) at 30°C.

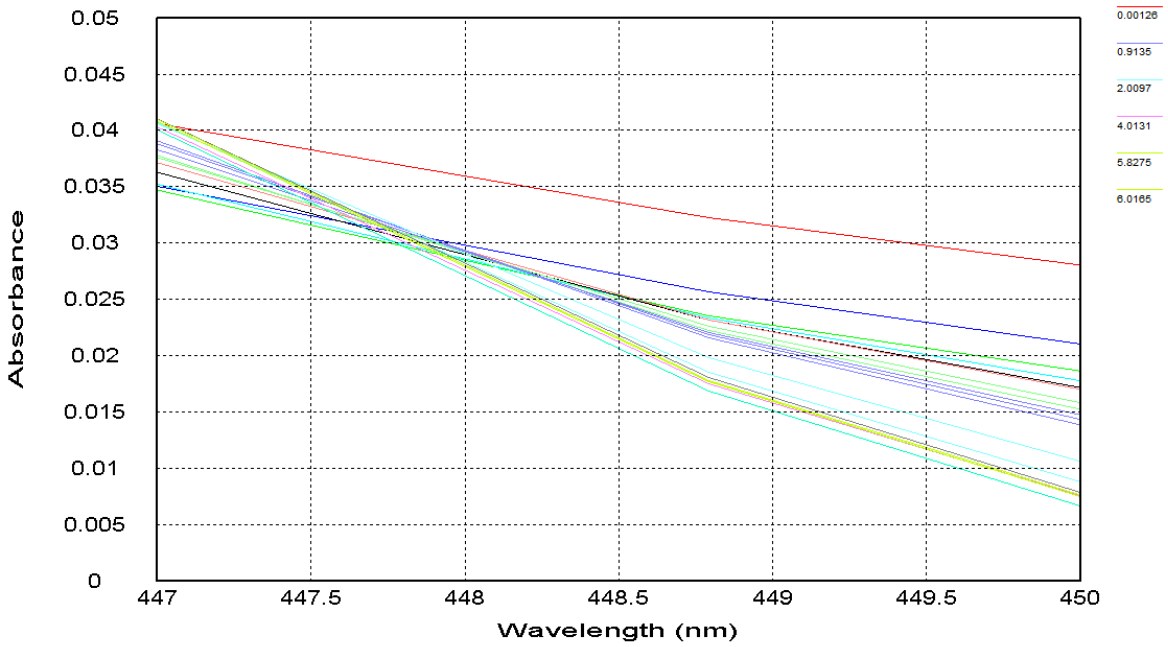

Figure 24. Pre steady-state spectral changes at isosbestic point of heme *b* (449 nm) of MtCDH upon reduction with cellobiose. Zoom in of **Figure 21**.

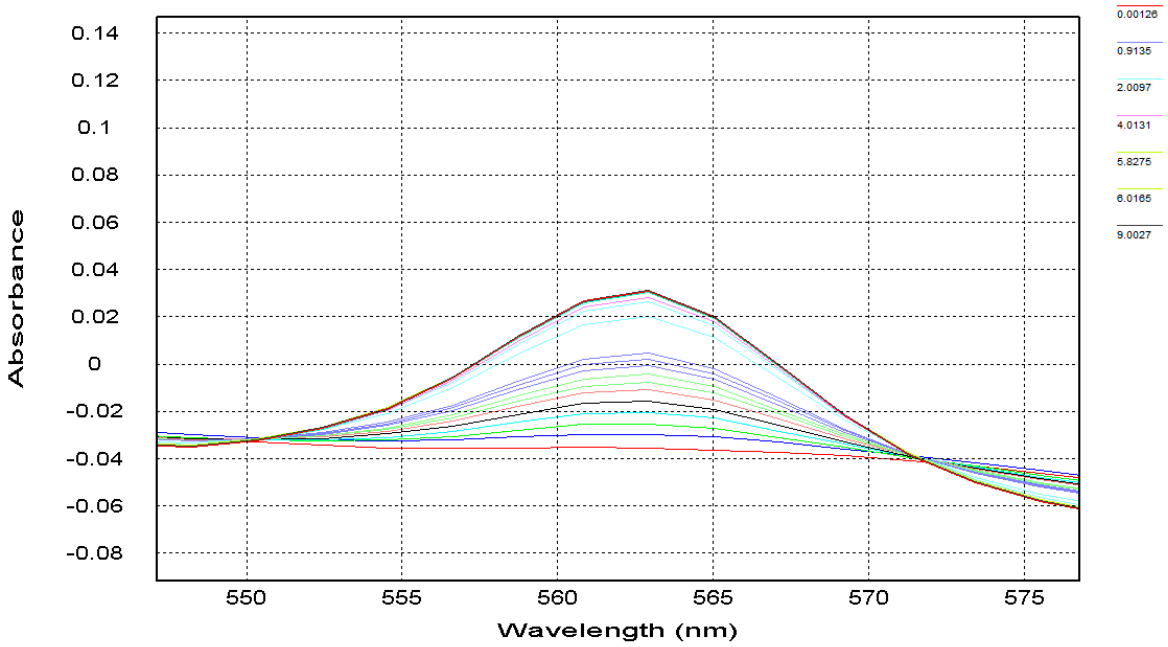

Figure 25. Pre steady-state spectral changes of heme *b* of *Mt*CDH at 562 nm upon reduction with cellobiose. Zoom in of Figure 21. No interference in absorption spectrum of FAD can be expected at this wavelength.

Since the rates for FAD reduction with both, cellobiose and lactose as substrates, appeared to be biphasic, they were fitted to double exponential curves yielding two rates, whereas the first one ($k_{obs}^{FAD\ fast}$) exhibits an average 20-fold faster reaction then the second rate($k_{obs}^{FAD\ slow}$).

Interestingly, $k_{obs}^{FAD\ slow}$ was minimal slower (an average of 15%) than $k_{obs}^{haem\ b}$ which showed an initial lag followed by a monophasic process. $k_{obs}^{FAD\ fast}$ is 21-fold faster than $k_{obs}^{haem\ b}$, when cellobiose or lactose are used as substrates (500 µM).

Different results in reduction behavior were obtained with glucose or maltose as substrates, the latter is a disaccharide consisting of two molecule glucose joined with an α-1,4 bond. Especially at low substrate concentrations (1.5, 5, 15 mM), FAD reduction seemed to follow a monophasic process and concomitantly exhibiting rates equal to $k_{obs}^{haem\ b}$, where no lag of the heme *b* rate was observed. These findings imply that the reduction of both prosthetic groups is happening independently from each other, unless substrate affinity is low. Consequently, it can be assumed that two reduction mechanisms at low substrate concentrations depending on the affinity of the substrate. Substrates with high affinity to the enzyme force induced fitting, followed by the reduction of the FAD. Only after the release of the substrate, the heme *b* is reduced and concomitantly FAD re-oxidized. Under low substrate concentration, substrates with low affinity to the enzyme do not fit properly, thus stochastic reduction of the two prosthetic groups, the FAD and the heme *b* cofactors, are happening independently from each other. An exceptional position takes glucose (500 mM) which contrary to maltose exhibits high rates for $k_{obs}^{FAD\ fast}$ and $k_{obs}^{haem\ b}$, 15.0 and 0.62 s^{-1}, respectively. The reason for this could lie in the fact that glucose is a rather small molecule (monosaccharide) compared to maltose which is a α-1,4 disaccharide. Thus, too big for efficient stochastically reduction and could moreover inhibit the reaction at high concentrations as it does not fit properly into the "β-1,4 disaccharide" binding site.

In Table 9 andTable 10, the observed rate constants and the derived limiting rate constants (k_{lim}) and dissociation constant (K_d) for cellobiose, lactose, glucose and mannose are summarized. Due to lack of data, the kinetic constants for FAD reduction rates of glucose were not determined. The substrates cellobiose and lactose show similar properties for both co-factors, but with cellobiose a significantly lower K_d is achieved. The catalytic efficiency of the heme *b* reduction process for glucose is outstanding, showing 3.2-fold higher values as with the natural substrate cellobiose. Maltose shows poor characteristics as a substrate for *Mt*CDH.

Table 9. Reduction rates of recombinant *Mt*CDH for various substrates. Stopped-flow measurements were performed with 5 µM enzyme at pH 4.5 in 100 mM citrate phosphate buffer.

substrate	$k_{obs}^{FAD\ fast}$	$k_{obs}^{FAD\ slow}$	$k_{obs}^{heme\ b}$	$k_{obs}^{FAD\ fast} / k_{obs}^{heme\ b}$	substrate	$k_{obs}^{FAD\ fast}$	$k_{obs}^{FAD\ slow}$	$k_{obs}^{heme\ b}$	$k_{obs}^{FAD\ fast} / k_{obs}^{heme\ b}$
cellobiose (µM)					***lactose (µM)***				
20	13.9	0.70	0.84	16.5	20	8.6	0.56	0.68	12.6
50	16.5	0.73	0.87	19.0	50	12.0	0.66	0.81	14.8
150	17.1	0.75	0.89	19.2	150	16.0	0.73	0.87	18.4
500	18.6	0.77	0.90	20.7	500	18.5	0.76	0.89	20.8
1500	17.8	0.78	0.91	19.6	1500	19.6	0.80	0.90	21.8
5000	17.6	0.79	0.90	19.6	5000	20.0	0.81	0.91	22.0
15000	17.7	0.78	0.90	19.7	15000	18.9	0.77	0.90	21.0
50000	16.8	0.75	0.85	19.8	50000	18.2	0.74	0.83	21.9
glucose (mM)					***maltose (mM)***				
1.5	0.04	n.d.	0.04	1.0	1.5	0.09	n.d.	0.08	1.1
5	0.08	n.d.	0.08	1.0	5	0.13	n.d.	0.14	0.9
15	0.17	n.d.	0.17	1.0	15	0.17	n.d.	0.18	0.9
50	1.8	0.23	0.35	5.1	50	1.0	0.14	0.20	4.9
150	9.0	0.45	0.56	16.1	150	2.5	0.17	0.18	13.9
500	15.0	0.54	0.62	24.2	500	2.3	0.15	0.15	15.3

Table 10. Limiting rate constants (k_{lim}) and dissociation constant (K_d) of *Mt*CDH for various substrates. The kinetic parameters were obtained from equation 15.

substrate	k_{lim}^{FAD} (s^{-1})	K_d^{FAD} (µM)	$k_{lim}^{FAD} / K_d^{FAD}$ (s^{-1} μM^{-1})	$k_{lim}^{heme\ b}$ (s^{-1})	$K_d^{heme\ b}$ (µM)	$k_{lim}^{heme\ b} / K_d^{heme\ b}$ (s^{-1} μM^{-1})
cellobiose	16.8	129.1	0.13	0.85	143.8	0.006
lactose	18.2	126.3	0.14	0.83	202.8	0.004
glucose	n.d.	n.d.	n.d.	0.67	35.6	0.019
maltose	2.9	1.1E+05	2.6E-05	0.15	6.5E+03	2.3E-05

3.3.2 pH Profile of *Mt*CDH with lactose as substrate

Pre steady-state kinetic experiments were carried out at different lactose concentrations (50, 500, 50000 µM) and pH values ranging from 3.0 to 7.5 (Table 11). The rate constant for FAD reduction at pH 3.0 upon 50 µM lactose was almost identical to the one of the heme *b* and no significant second phase of lag of heme *b* was observed.

The pH Profile in Figure 26 shows clearly that with increasing pH observed rate constants for the FAD increase, whereas the observed rates for heme *b* increase until pH 4.0 (500 and 50000 µM lactose) and 4.5 (50 µM lactose) where they reach maximum rate constants of 0.93 and 0.81 s^{-1}, respectively. Beyond pH 4.5, the observed rate constants for heme *b* at different lactose concentrations coincide while rapidly falling. At neutral pH, very little reduction of the heme *b* was observed. The rate constants for FAD at very low lactose concentration (50 µM) are increasing from very little to the observed rate constant of 20 s^{-1} over the whole pH range. Beyond pH 4.0, the observed rate constants for FAD of higher lactose concentrations also coincide and a maximum rate constant of approximately 38 s^{-1} is reached at neutral pH.

Table 11. Pre steady-state observed rate constants. Reduction of *Mt*CDH (5µM) upon lactose oxidation (50, 500, 50000 µM) at various pH (100 mM citrate phosphate buffer).

pH	k_{obs}^{FAD}			$k_{obs}^{heme\ b}$		
	50 µM	500 µM	50000 µM	50 µM	500 µM	50000 µM
3.0	0.18	4.8	11.6	0.15	0.48	0.70
3.5	2.5	10.7	15.0	0.43	0.77	0.87
4.0	8.5	16.5	17.0	0.73	0.93	0.93
4.5	12.0	18.5	18.2	0.81	0.89	0.83
5.0	11.8	18.0	18.6	0.55	0.58	0.55
5.5	14.0	20.3	21.7	0.29	0.30	0.28
6.0	13.8	26.9	27.6	0.15	0.15	0.14
7.0	19.2	37.8	38.0	0.07	0.07	0.06
7.5	18.9	38.4	37.5	0.05	0.05	0.05

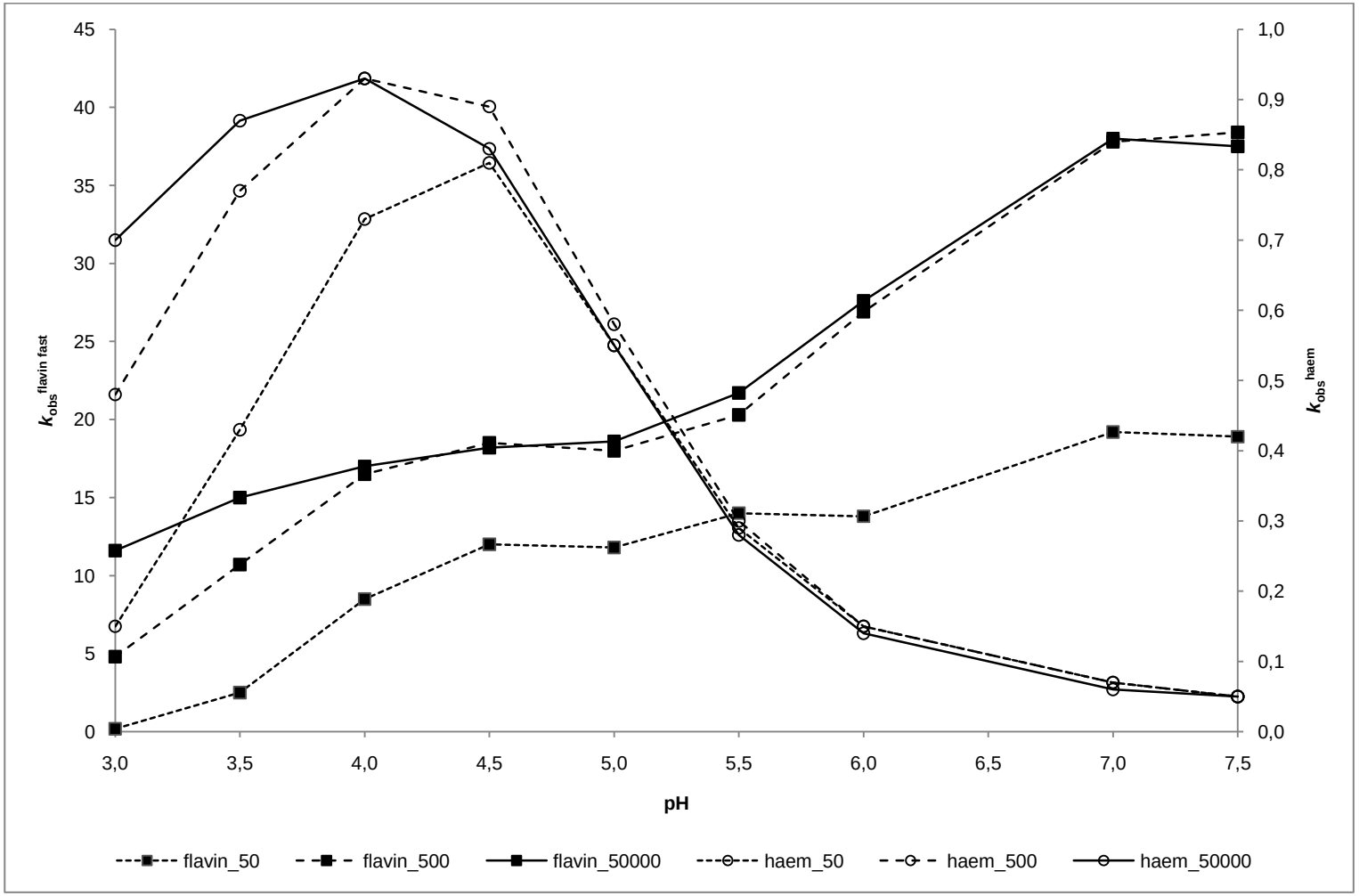

Figure 26. pH Profile of *Mt*CDH upon mixing with lactose at different concentrations.

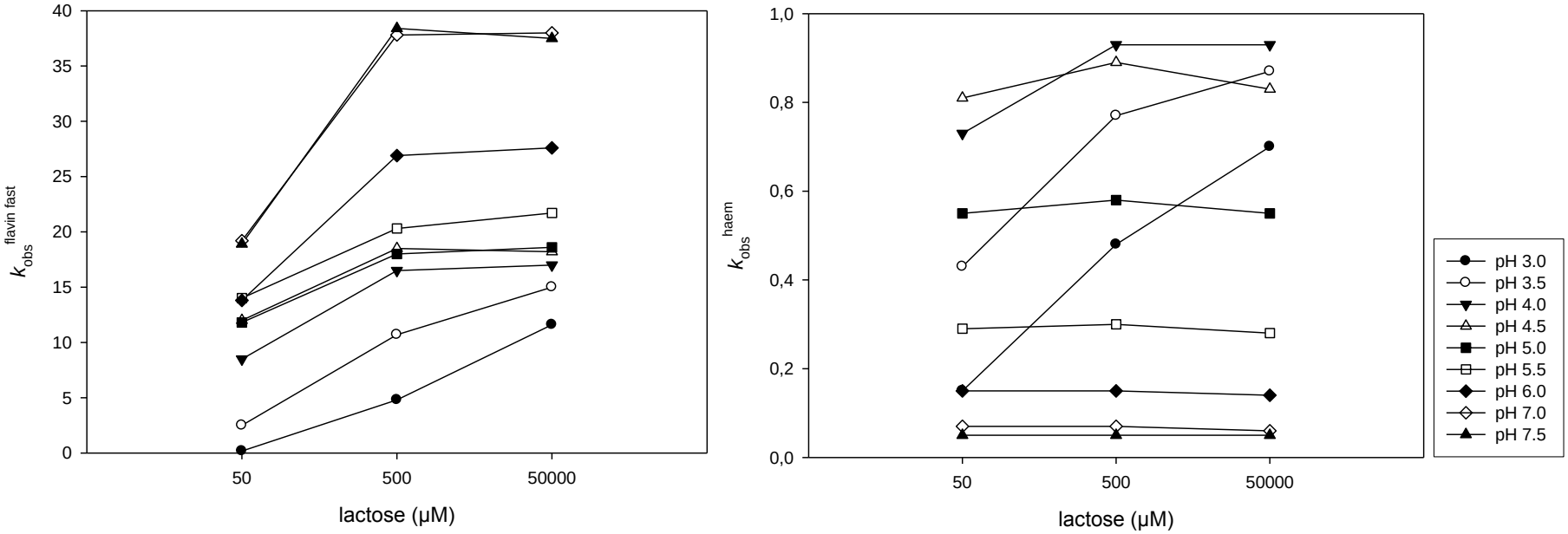

Figure 27. Observed rate constants for FAD (fast phase) and heme *b* upon reduction with lactose.

3.3.3 Pre steady-state kinetics of surface-charge recombinant *Mt*CDH variants

Table 12 shows the observed rate constants for the recombinant wild-type *Mt*CDH and its variants upon lactose and glucose reduction. As already discussed, the observed reduction rates for FAD are increasing with increasing pH, whereas for heme *b*, the rates decreased with increasing pH. The purpose of designing mutants of *cdh* was to create variants, which exhibit a higher rate for IET while leaving FAD reduction unaffected at neutral pH. As already mentioned in 1.9 the design principle was the exchange of negatively charged amino acids on the flavodehydrogenase domain with neutral or positively charged ones to reduce electrostatic repulsion.

The following presentation of results concentrates on the reduction rates upon 500 µM lactose and 50 mM glucose at pH 7.5, unless otherwise noted. The relative absorption changes of FAD ($\Delta_{510\ nm\ -\ 483\ nm}$) and heme *b* ($\Delta_{572\ nm\ -\ 562\ nm}$) of the variants were compared with those of the wild-type enzyme (Figure 28). D547K exhibits 2.4-fold (lactose) and 1.8-fold (glucose) higher rate constants for heme *b* reduction while showing no significant increase for the FAD. Mutant E550K also showed slightly higher rate constants for heme *b* (1.4-fold for lactose, no effect for glucose) and no significant changes on FAD reduction rates.

The combination of both mutations, in the variant D547K/E550K shows a 3.6-fold increase of the heme *b* reduction rate. Its performance in reduction, especially upon glucose is outstanding. A 2.8-fold increase for the observed reduction rate of heme *b* was found. Reduction rates for the FAD showed no significant changes compared to the recombinant wild-type *Mt*CDH. This makes the variant D547K/E550K the most promising for further research, not only for its outstanding features on heme *b* reduction rates in general, but also for its performance with glucose in particular. Figure 29 shows relative absorption plotted versus time for D547K/E550K, for both substrates lactose and glucose at pH 4.5 and pH 7.5. Comparison with recombinant wild-type *Mt*CDH clearly shows the high reduction rate of D547K/E550K upon glucose at neutral pH. The gap between the relative absorption curves narrows, whereas the reduction rate for FAD shows not that typical double-sigmoid shape behavior as in the wild-type. While the mutation leads to a 10-fold faster reduction process upon lactose at acidic and neutral pH, the reduction velocity for both FAD and heme *b* are only marginally affected at acidic pH upon

glucose. The reason behind is that the mutant was designed to show higher heme *b* rates at neutral pH where the wild-type enzyme shows only poor reduction of heme *b*.

Figure 28 and Figure 29 show the relative absorption changes of recombinant wild-type *Mt*CDH and D547K/E550K. The FAD curve has a double-sigmoid shaped curve. It can be assumed that after the FAD reaches a plateau, the heme *b* reduction might interfere in shifting the FAD curve further upwards.

Problems were faced when evaluating the observed rate constants for the triple and quadruple mutated variants, D547K/E550K/E603K and D297K/D547K/E550K/E603K respectively. Thus, the observed rate constants listed in

Table 12 must be considered with caution. The reduction behavior of these mutants is plotted in Figure 30 andFigure 31. The following discussions concerns experiments carried out at pH 7.5. For both mutants upon reduction of lactose as well as glucose, the observed reduction curves for FAD are lower than in the wild-type enzyme; 65, 75, 58 and 40% reduction was achieved after 1 s upon mixing with lactose for wild-type, D547K/E550K, D547K/E550K/E603K and D297K/D547K/E550K/E603K respectively. Similar reduction behavior for FAD is achieved upon glucose as the substrate. The reduction process for heme *b* on the other hand is similar to the mutant D547K/E550K; 40, 80 and 70% reduction after 10 s upon reduction of either substrates for wild-type, D547K/E550K/E603K and D297K/D547K/E550K/E603K respectively. Thus, D547K/E550K/E603K and D297K/D547K/E550K/E603K show similar reduction features as D547K/E550K for heme *b* in CDH but lower rates for FAD reduction.

Table 12. Observed rate constants for FAD (fast phase) and heme *b* of wild-type *Mt*CDH and variants.

	variant	pH	k_{obs}^{FAD}	$k_{obs}^{heme\ b}$	variant	pH	k_{obs}^{FAD}	$k_{obs}^{heme\ b}$
50 µM lactose	wt	4.5	12.0	0.81	2	4.5	9.4	1.3
500 µM lactose			18.5	0.89			17.3	1.6
5 mM glucose			0.08	0.08			0.13	0.13
50 mM glucose			1.8	0.35			3.5	0.61
50 µM lactose	wt	7.5	18.9	0.05	2	7.5	16.3	0.18
500 µM lactose			38.4	0.05			40.4	0.18
5 mM glucose			1.1	0.05			1.6	0.12
50 mM glucose			6.9	0.06			8.0	0.17
50 µM lactose	1D	4.5	10.6	1.2	3	4.5	0.10	0.05
500 µM lactose			18.7	1.4			0.18	0.19
5 mM glucose			0.14	0.11			0.04	0.04
50 mM glucose			1.6	0.53			0.19	0.21
50 µM lactose	1D	7.5	18.3	0.12	3	7.5	2.1	0.07
500 µM lactose			43.4	0.12			3.2	0.16
5 mM glucose			1.5	0.08			2.4	0.08
50 mM glucose			7.4	0.11			3.3	0.15
50 µM lactose	1E	4.5	11.6	0.78	4	4.5	n.d.	0.03
500 µM lactose			18.0	0.88			0.08	0.09
5 mM glucose			0.18	0.07			n.d.	0.03
50 mM glucose			1.4	0.34			0.09	0.11
50 µM lactose	1E	7.5	19.6	0.07	4	7.5	0.14	0.07
500 µM lactose			40.9	0.07			1.3	0.14
5 mM glucose			1.1	0.05			0.09	0.06
50 mM glucose			6.7	0.06			1.3	0.16

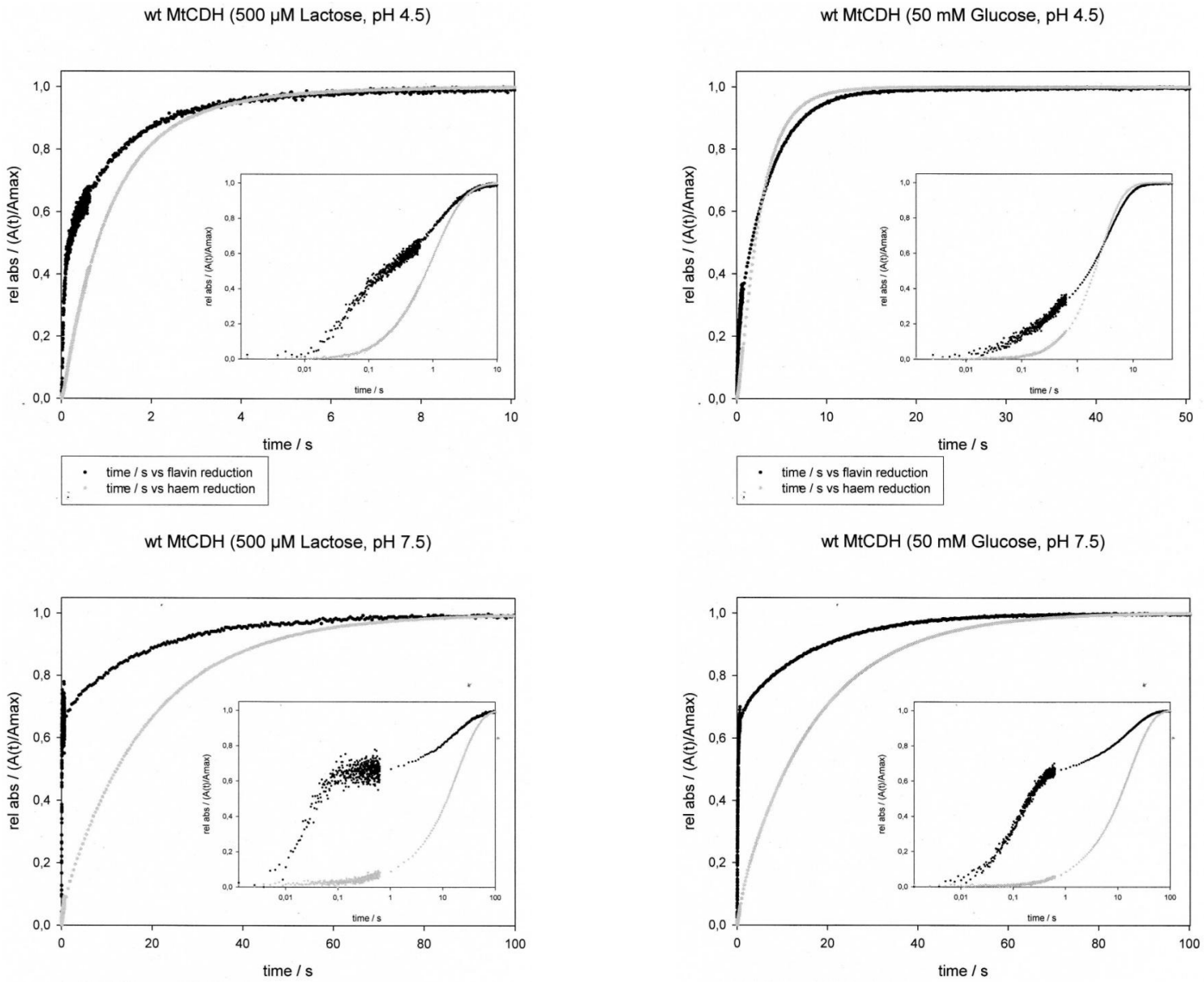

Figure 28. Relative absorption changes of recombinant wild-type *Mt*CDH upon reduction lactose and glucose at pH 4.5 and 7.5.

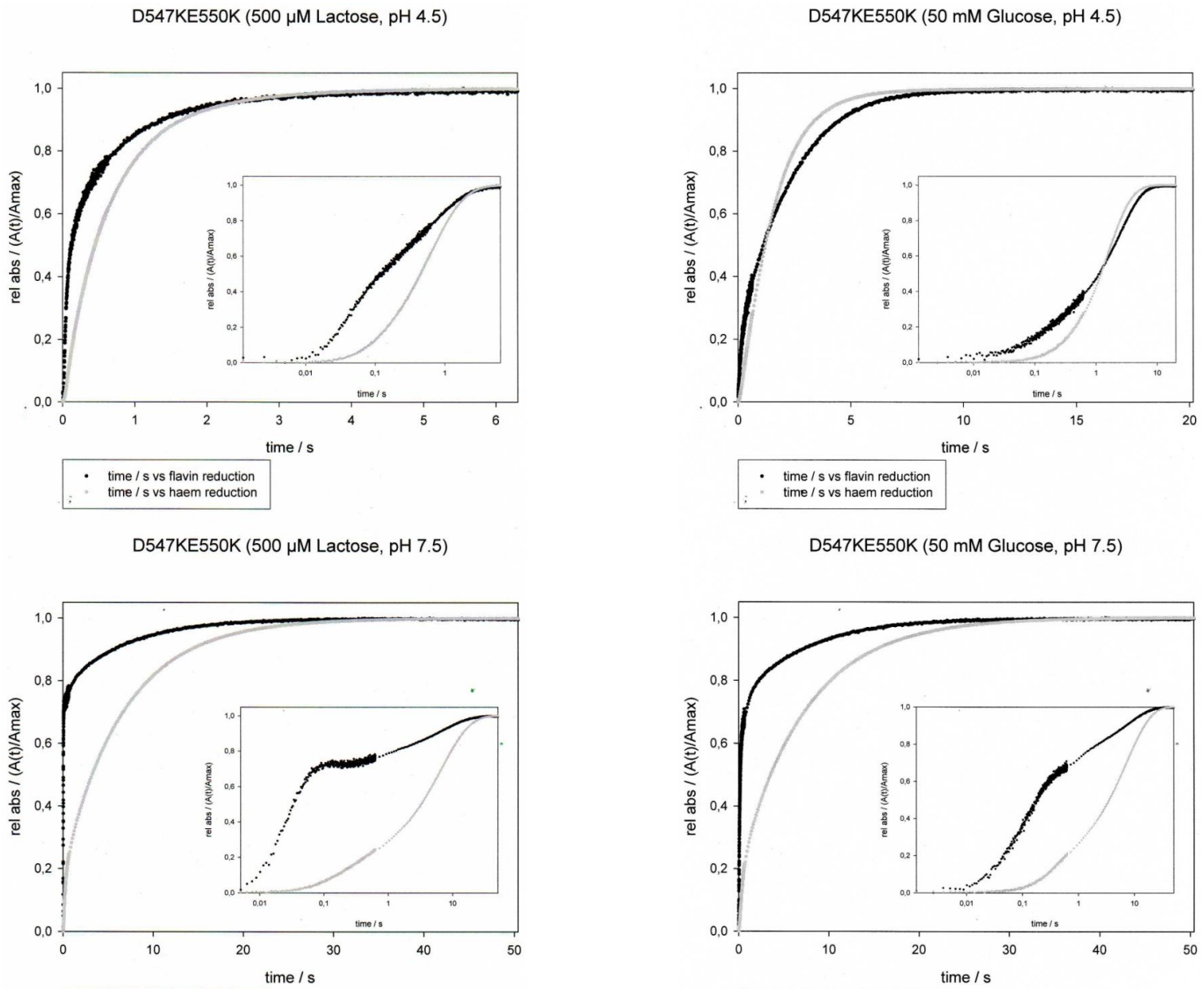

Figure 29. Relative absorption changes of recombinant *Mt*CDH variant D547K/E550K upon reduction lactose and glucose at pH 4.5 and 7.5.

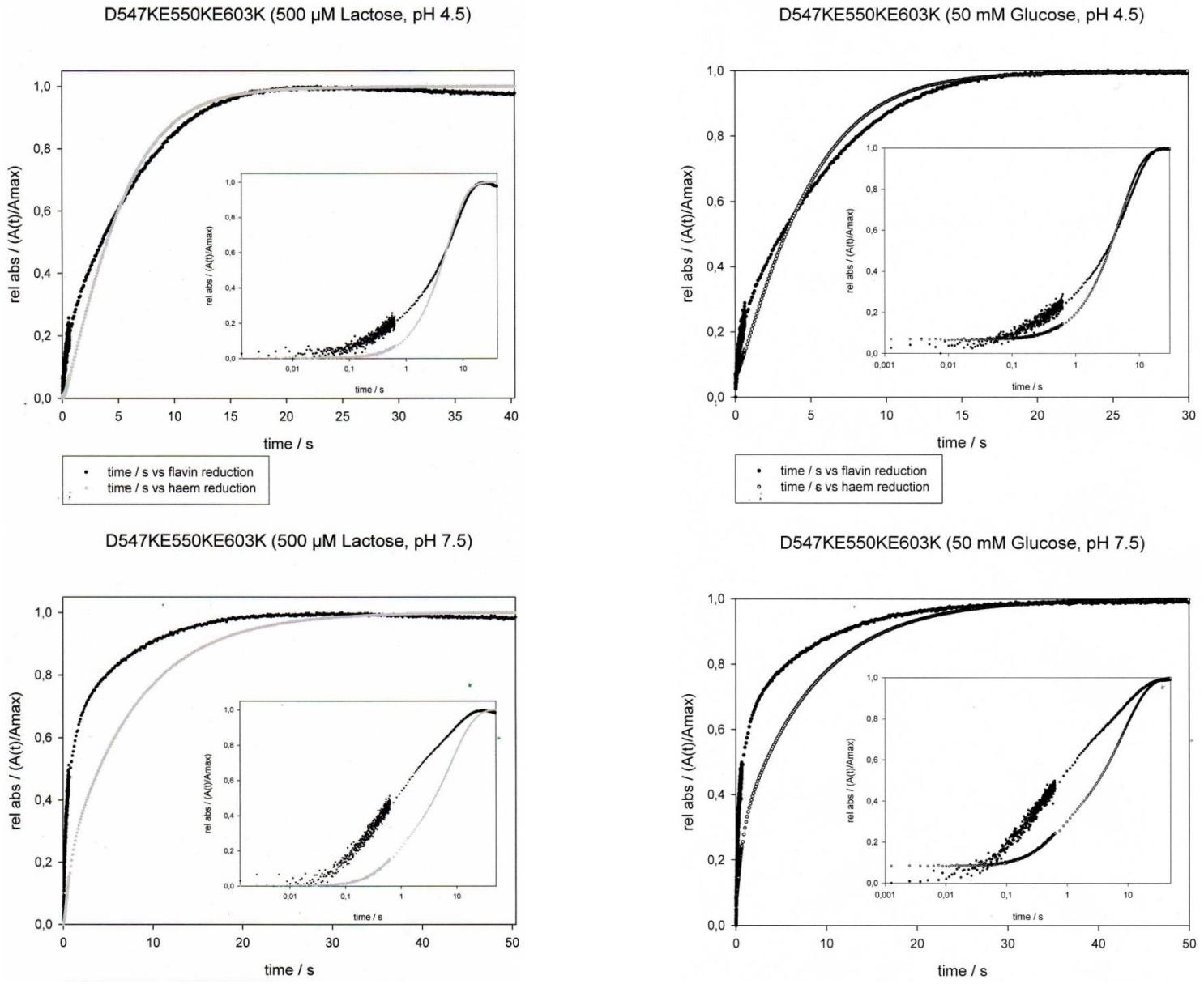

Figure 30. Relative absorption changes of recombinant *Mt*CDH variant D547K/E550K/E603K upon reduction lactose and glucose at pH 4.5 and 7.5.

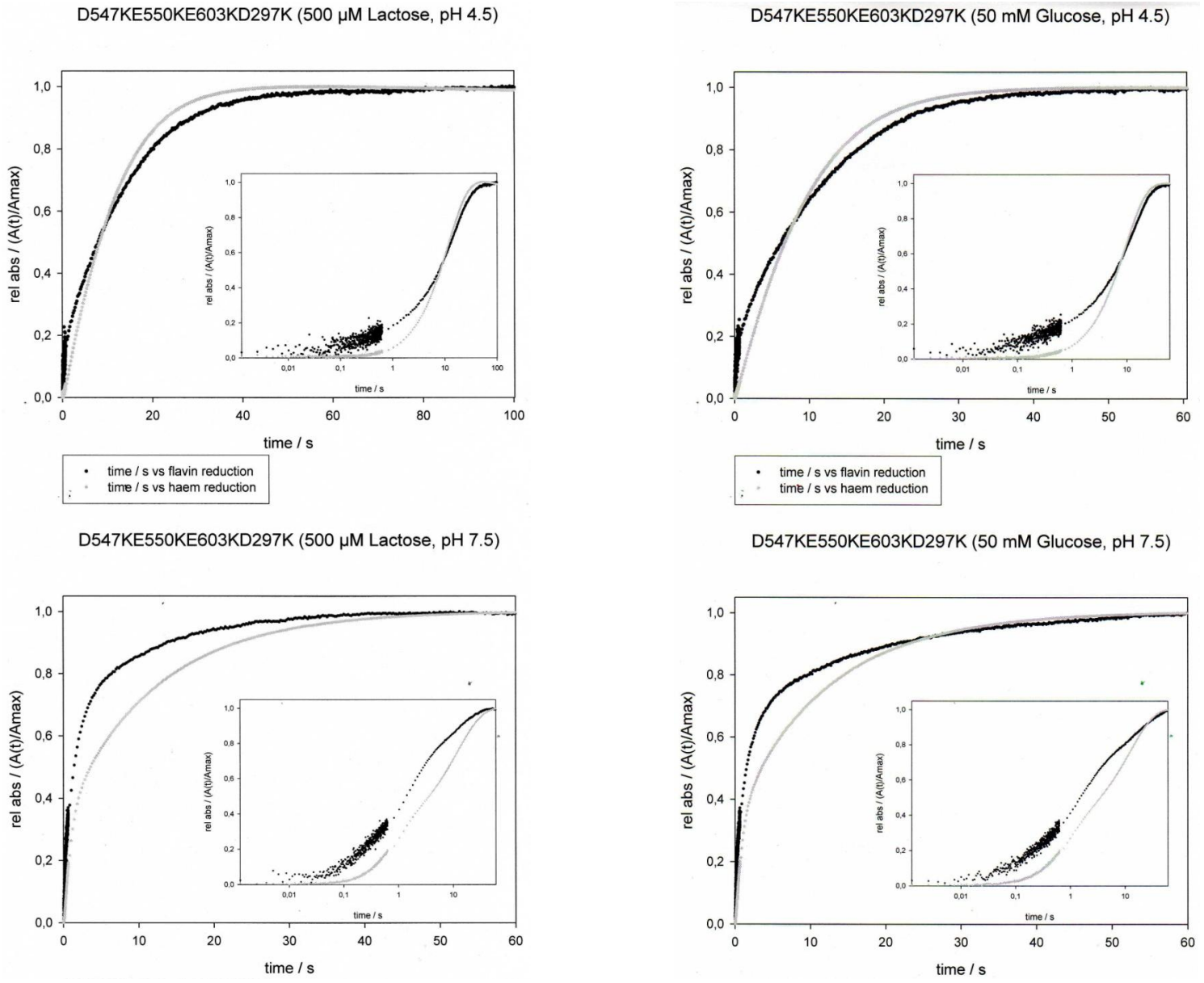

Figure 31. Relative absorption changes of recombinant *Mt*CDH variant D297K/D547K/E550K/E603K upon reduction lactose and glucose at pH 4.5 and 7.5.

3.3.4 Studies with recombinant *Pc*CDH

The reduction of the holoenzyme for recombinant wild-type and recombinant deglycosylated *Pc*CDH was completed within 1 s and no lag phase of the heme *b* was observed (**Fehler! Verweisquelle konnte nicht gefunden werden.**). Deglycosylated *Pc*CDH showed 11 and 12% lower reduction rates than glycosylated *Pc*CDH for the FAD and heme *b* prosthetic groups, respectively. However, it is not fully clear if this can be ascribed to degradation processes of deglycosylated *Pc*CDH which is more vulnerable to such than glycosylated enzymes.

Experiments with recombinant wild-type and recombinant deglycosylated *Pc*CDH showed approximately 3.8-fold and 18.2-fold higher reduction rates for the prosthetic FAD and heme *b*, respectively , than *Mt*CDH (Table 13). The reduction rate of the heme *b* thus is only 4.5-fold slower than the FAD rate, compared to 21.9-fold with *Mt*CDH. As with *Mt*CDH the slower rate of the double exponential fitting is slightly slower than the rate for heme *b* reduction.

Table 13. Observed rate constants for *Mt*CDH and *Pc*CDH (glycosylated and deglycosylated). Stopped flow measurements were performed with 5 µM enzyme against 50 mM lactose at pH 4.5 in 100 mM sodium acetate buffer.

	$k_{obs}^{\text{FAD fast}}$	$k_{obs}^{\text{FAD slow}}$	$k_{obs}^{\text{heme } b}$	$k_{obs}^{\text{FAD fast}} / k_{obs}^{\text{heme } b}$
glycosylated *Pc*CDH	72.5	15.6	16.1	4.5
deglycosylated *Pc*CDH	64.3	12.9	14.1	4.6
***Mt*CDH**	18.2	0.74	0.83	21.9

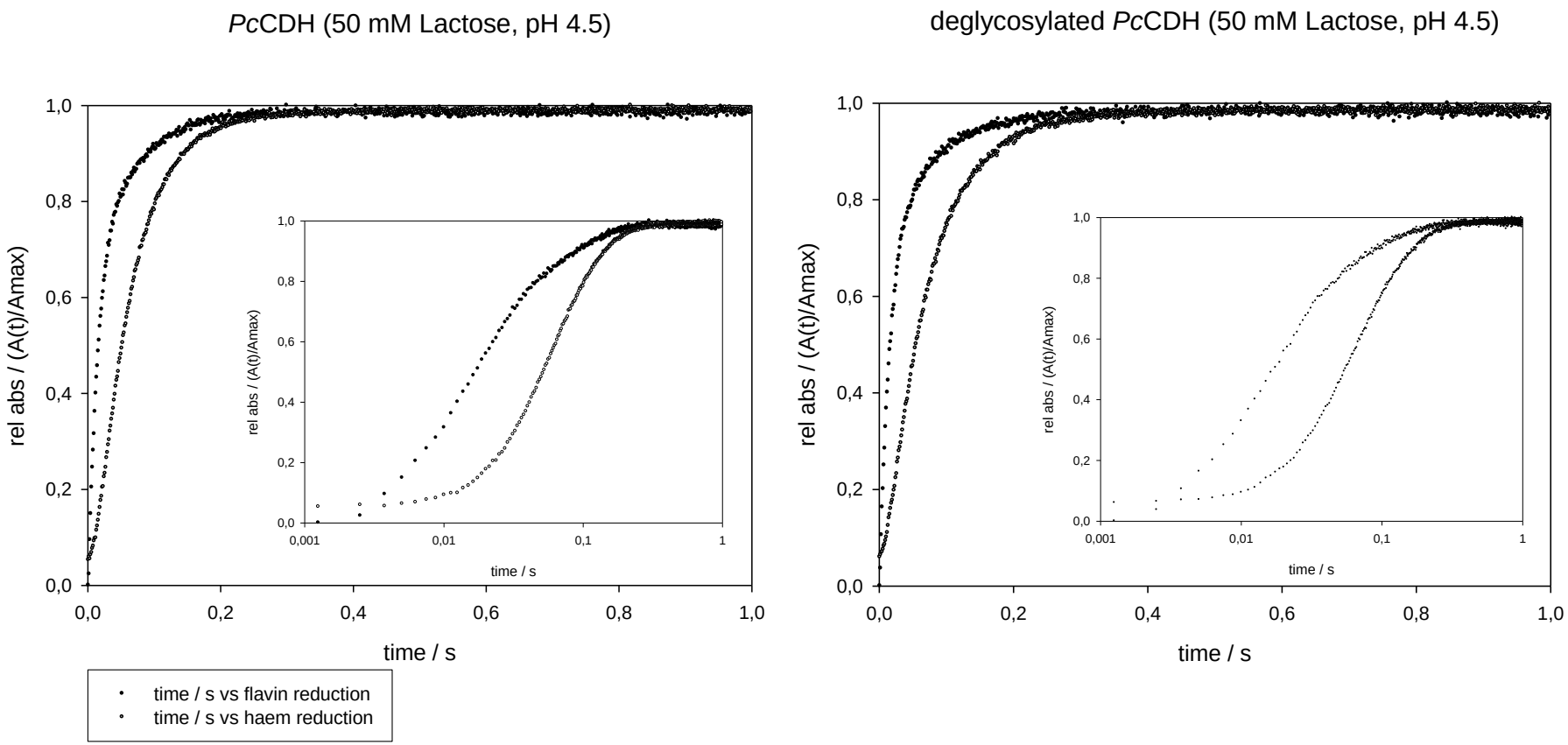

Figure 32. Relative absorption changes of recombinant *Pc*CDH and deglycosylated *Pc*CDH upon reduction with lactose at pH 4.5.

4 Summary

Heterologous expression and purification of *Myriococcum thermophilum* CDH in *Pichia pastoris* formed the basis of this study. The highly purified enzyme with a A_{420}/A_{280} ratio of 0.64 was then subjected to pre steady-state analysis. The catalytic efficiencies for FAD and heme *b* for cellobiose, lactose, glucose and maltose were determined. The substrates cellobiose and lactose show similar rate constants for both co-factors, but with cellobiose a significantly lower K_d value was achieved. The catalytic efficiency of the heme *b* reduction process for glucose is outstanding, showing 3.2-fold higher value as with the natural substrate cellobiose. Maltose showed very poor characteristics as a substrate. The highest observed rate constant of the heme *b* was 0.93 s^{-1} at pH 4.0, whereas for FAD the highest observed rate constant was 38.0 s^{-1} at pH 7.0, upon lactose reduction (50 mM).

D547K/E550K and D547K/E550K/E603K were found to be the most promising surface-charge variants, as they exhibit satisfying reduction performance of FAD with more than 3-fold increased heme *b* rate constants. Here, only the relevant observations upon glucose reduction at neutral pH are summarized. The observed reduction curves for FAD were lower, while the rates for heme *b* were significantly higher than observed for the wild-type enzyme. After 1 s upon mixing enzyme with the substrate, the FAD showed 65% reduction of the wild-type *Mt*CDH, 75% reduction of the D547K/E550K and 58% reduction of the D547K/E550K/E603K. After 10 s upon mixing, heme *b* was reduced by 60% in D547K/E550K, 80% in D547K/E550K/E603K and 70% in D297K/D547K/E550K/E603K, whereas the wild-type enzyme only exhibited a 40% reduction of heme *b*. Thus, D547K/E550K/E603K and D297K/D547K/E550K/E603K show similar reduction features as D547K/E550K for heme *b* in CDH but lower rates for FAD reduction.

The reduction of the holoenzyme upon 50 mM lactose for recombinant wild-type and recombinant deglycosylated *Pc*CDH was completed within 1 s and no lag phase of the heme *b* was observed. Deglycosylated *Pc*CDH showed 11 and 12% lower reduction rates than glycosylated *Pc*CDH for the FAD and heme *b* prosthetic groups, respectively. It can be assumed that deglycosylation of the enzyme makes it more unstable and accounts for lower reduction rates. Recombinant wild-type and recombinant deglycosylated *Pc*CDH showed approximately 3.8-fold and 18.2-fold higher reduction rates than *Mt*CDH for the prosthetic FAD and heme *b*,

respectively. The reduction rate of the heme *b* thus is only 4.5-fold slower than the FAD rate, compared to 21.9-fold with *Mt*CDH.

As surface-charge variants of CDH from *Myriococcum thermophilum*, showed little glucose discrimination and outstanding reduction rates for heme *b*, they have the potential to become promising tools for biotechnological applications, such as enzymatic fuel cells or in the medical-diagnostic area as glucose biosensors.

References

1. **Crawford, J.H.** Composting of agricultural wastes - a review. *Process Biochem.* 1983, 18: 14-18.

2. **Tuomela, M., Vikman, M., Hatakka, A., Itävaara, M.** Biodegradation of lignin in a compost environment: a review. *Biores Technol.* 2000, 72:169-83.

3. **Maheshwari, R., Bharadwaj, G., Bhat, M.K.** Thermophilic fungi: their physiology and enzymes. *Micorbiol Mol Biol Rev.* 2000, 64.3:461-88.

4. **Cameron, M.D., Aust, S.D.** Degradation of chemicals by reactive radicals produced by cellobiose dehydrogenase from *Phanerochaete chrysosporium*. *Arch Biochem Biophys.* 1999, 376:115–21.

5. **Li, B., Nagalla, S.R., Renganathan, V.** Cloning of a cDNA encoding cellobiose dehydrogenase, a hemoflavoenzyme from *Phanerochaete chrysosporium*. *Appl Environ Microbiol.* 1996, 62:1329–35.

6. **Moukha, S.M., Dumonceaux, T.J, Record, E., Archibald, F.S.** Cloning and analysis of *Pycnoporus cinnabarinus* cellobiose dehydrogenase. *Gene.* 1999, 234: 23-33.

7. **Cameron, M.D., Aust, S.D.** Cellobiose dehydrogenase - an extracellular fungal flavocytochrome. *Enzyme Microb Technol.* 2001, 28:129-38.

8. **Westermark, U., Eriksson, K.E.** Cellobiose:quinone oxidoreductase, a new wood-degrading enzyme from white-rot fungi. *Acta Chem Scand.* 1974, B28:209–14.

9. **Hallberg, B.M., Bergfors, T., Bäckbro, K., Pettersson, G., Henriksson, G., Divne, C.** A new scaffold for binding haem in the cytochrome domain of the extracellular flavocytochrome cellobiose dehydrogenase. *Structure 2000.* 2000, 8:79–88.

10. **Hallberg, B.M., Henriksson, G., Pettersson, G., Divne, C.** Crystal structure of the flavoprotein domain of the extracellular flavocytochrome cellobiose dehydrogenase. *J Mol Biol.* 2002, 315(3):421-34.

11. **Zámocký, M., Ludwig, R., Peterbauer, C., Hallberg, B.M., Divne, C., Nicholls, P., Haltrich, D.** Cellobiose dehydrogenase - a flavocytochrome from wood-degrading, phytopathogenic and saprotrophic fungi. *Curr Protein Pept Sci.* 2006, 7:255-80.

12. **Berg, J.M., Tymocko, J.L., Stryer, L.** *Biochemistry 5th Edition.* New York : W. H. Freeman and Company, 2002.

13. **Price, N.C., Dwek, R.A., Wormald, M., Ratcliffe, R.G.** *Principles and problems in physical chemistry for biochemists.* Oxford University Press, 2001.

14. **Wilson, M.T., Torres, J.** Stopped-flow spectroscopy. M.G. Gore. *Spectrophotometry and spectrofluorimetry - A practical approach.* s.l. : Oxford University Press, 2000.

15. **Henriksson, G., Johansson, G., Pettersson, G.** A critical review of cellobiose dehydrogenases. *J Biotechnol.* 2000, 78:93-113.

16. **Igarashi, K., Momohara, I., Nishino, T., Samejima, M.** Kinetics of inter-domain electron transfer in flavocytochrome cellobiose dehydrogenase from the white-rot fungus *Phanerochasete chrysosporium*. *Biochem J.* 2002, 365: 521-26.

17. **Igarashi, K., Yoshida, M., Matsumura, H., Nakamaru, N., Ohno, H., Samejima, M., Nishino, T.** Electron transfer chain reaction of the extracellular flavocytochrome cellobiose dehydrogenase from the basidiomycete *Phanerochaete chrysosporium*. *FEBS J.* 2005, 272:2869-77.

18. **Cameron, M.D., Timofeevski, S., Aust, S.D.** Enzymology of *Phanerochaete chrysosporium* with respect to the degradation of recalcitrant compounds and xenobiotics. *Appl Microbiol Biotechnol.* 2000, 54: 751-58.

19. **Mason, M.G., Nicholls, P., Divne, C., Hallberg, B.M., Henriksson, G., Wilson, M.T.** The heme domain of cellobiose oxidoreductase: a one-electron reducing system. *Biochim Biophys Acta.* 2003, 1604:47– 54.

20. **Kittl, R., Harreither, W., Nicholls, P., Gorton, L., Haltrich, D., Ludwig, R.** Characterisation of cellobiose dehydrogenase from the ascomycete *Myriococcum thermophilum*, manuscript in preparation.

21. **Zámocký, M., Schümann, C., Sygmund, C., O'Callaghan, J., Dobson, A.D.W., Ludwig, R., Haltrich, D., Peterbauer, C.** Cloning, sequence analysis and heterlogous expression in Pichia pastoris of a gene encoding a thermostable cellobiose dehydrogenase from *Myriococcum thermophilum*. *Prot Express Purif.* 2008, 59:258-65.

22. **Schenkenfelder, J.** Cloning, expression and characterisation of cellobiose dehydrogenase variants of ascomycetous and basidiomycetous sources for third generation biosensors. *University of Natural Resources and Life Sciences, Vienna.* 2010. Master thesis.

23. **Invitrogen (TM) life technologies.** Pichia fermentation process guidelines. [Online] Version B, 053002. http://www.molecularinfo.com/MTM/G/G2/G2-9.pdf.

24. **Bradford, M.** A rapid and sensitive method for the quantitation of microgram quantities of protein utilizing the principle of protein-dye binding. *Anal Biochem.* 1976, 72: 248-54.

25. **Baminger, U., Subramaniam, S. S., Renganathan, V., Haltrich, D.** Purification and characterization of cellobiose dehydrogenase from the plant pathogen *Sclerotium (Athelia) rolfsii*. *Appl Environ Microbiol.* 67: 1766-74.

26. **Palfey, B.A.** Time resolved spectral analysis. K.A. Johnson. *Kinetic analysis of macromolecules.* Oxford University Press, 2003.

27. **Narciso, M.** Purification, characterization and cloning of cellobiose dehydrogenase from ascomycete fungi. *University of Natural Resources and Life Sciences, Vienna.* 2010. Master thesis.

28. **Rouvière, N., Mayer, M., Tegoni, M., Capeillère-Blandin, C., Lederer, F.** Molecular interpretation of inhibition by excess substrate in flavocytochrome b_2: a study with wild-type and Y143F mutant enzymes. *Biochemistry.* 36: 7126-35.

29. **Bao, W., Usha, S., Renganathan, V.** Purification and characterization of cellobiose dehydrogenase, a novel extracellular hemoflavoenzyme from the white-rot fungus *Phanerochaete chrysosporium*. *Arch Biochem Biophys.* 1993, 300:705-13.